

1 **Crystal structures of *Arabidopsis* and *Physcomitrella* CR4 reveal the molecular architecture**
2 **of CRINKLY4 receptor kinases.**

3

4 Authors: Satohiro Okuda^{1,*}, Ludwig A. Hothorn^{2,#}, Michael Hothorn^{1,+}

5

6 Affiliations:

7 ¹Structural Plant Biology Laboratory, Department of Botany and Plant Biology, University of
8 Geneva, 1211 Geneva, Switzerland.

9 ²Institute of Biostatistics, Leibniz University, 30167 Hannover, Germany.

10 *present address: Department of Biological Science, School of Science, University of Tokyo, 113-
11 0033 Tokyo, Japan.

12 [#]retired.

13 ⁺To whom correspondence should be addressed: michael.hothorn@unige.ch

14

15 ORCIDs:

16 Satohiro Okuda: 0000-0001-6172-2515

17 Ludwig A. Hothorn 0000-0002-5162-1486

18 Michael Hothorn: 0000-0002-3597-5698

19 **Abstract**

20 **Plant-unique receptor kinases harbor conserved cytoplasmic kinase domains and sequence-**
21 **diverse ectodomains. Here we report crystal structures of CRINKLY4-type ectodomains from**
22 **Arabidopsis ACR4 and *Physcomitrella patens* PpCR4 at 1.95 Å and 2.70 Å resolution,**
23 **respectively. Monomeric CRINKLY4 ectodomains harbor a N-terminal WD40 domain and a**
24 **cysteine-rich domain (CRD) connected by a short linker. The WD40 domain forms a seven-**
25 **bladed β-propeller with the N-terminal strand buried in its center. Each propeller blade is**
26 **stabilized by a disulfide bond and contributes to the formation of a putative ligand binding**
27 **groove. The CRD forms a β-sandwich structure stabilized by six disulfide bonds and shares**
28 **low structural homology with tumor necrosis factor receptor domains. Quantitative binding**
29 **assays reveal that ACR4 is not a direct receptor for the peptide hormone CLE40. An ACR4**
30 **variant lacking the entire CRD can rescue the known *acr4-2* mutant phenotype, as can**
31 **expression of PpCR4. Together, an evolutionary conserved signaling function for CRINKLY4**
32 **receptor kinases is encoded in its WD40 domain.**

32 Introduction

33 Plants have evolved a unique set of membrane receptor kinases (RKs) that regulate diverse
34 aspects of growth and development, form the first layer of the plant immune system and mediate
35 symbiotic interactions. RKs contain a single membrane-spanning helix, a conserved dual-specificity
36 cytoplasmic kinase domain and sequence-diverse extracellular domains (ectodomains) involved in
37 signal perception and receptor activation¹. The three-dimensional structures and functions of plant
38 RKs with leucine-rich repeat (LRR) ectodomains have been characterized in detail, yielding a
39 molecular understanding of their ligand binding and receptor activation mechanisms².

40 Crystal structures of non-LRR RKs have been reported for lysine-motif domain containing
41 immune and symbiosis receptors involved in the perception of N-acetyl-D-glucosamin-containing
42 ligands³⁻⁵. S-locus receptor kinases involved in self recognition during flower pollination have been
43 structurally characterized to contain β -barrel lectin domains and growth factor-like domains, all
44 contributing to the specific recognition of a cysteine-rich signaling peptide⁶. Two other classes of
45 RKs with lectin domain-containing extracellular domains have subsequently been characterized⁷:
46 The CYSTEINE-RICH RECEPTOR-LIKE PROTEIN KINASES (CRKs) contain a tandem
47 arrangement of DOMAIN OF UNKNOWN FUNCTION 26 (DUF26) lectin domains, which may
48 be involved in the recognition of a carbohydrate ligand⁸. The *Catharanthus roseus* receptor kinase
49 1-like (CrRLK1L) family contains a tandem arrangement of malectin domains⁹ involved in the
50 sensing of cysteine-rich RAPID ALKALINIZATION FACTOR peptides¹⁰, which can be distinctly
51 bound to either LORELEI-like GLYCOLPHOSPHATIDYLINOSITOL (GPI)-ANCHORED
52 PROTEINS¹⁰ or to the LRR domains of extensins¹¹.

53 Plant-unique CRINKLY4 (CR4) -type RKs show an unusual ectodomain structure radically
54 different from the known LRR, LysM and lectin receptor kinases described above. The founding
55 member of this family was identified by mapping the *crinkly4* mutation affecting leaf epidermis
56 differentiation in maize¹². The putative receptor kinase CR4 was initially shown to contain an active
57 cytoplasmic protein kinase module as well as an ectodomain with distant sequence homology to
58 tumor necrosis factor receptor (TNFR) domains^{12,13}. TNFR type I and II receptors contain a
59 cysteine-rich ectodomain that folds into several ~40 amino-acid segments. Each segment contains 6
60 conserved cysteines engaged in disulfide bonds¹⁴ and can act as binding sites for growth factors¹⁵.
61 The sequence similarities between the CRINKLY4 and TNFR ectodomains suggested a role for
62 maize CR4 in growth factor-triggered cell differentiation responses^{13,16}. Anti-sense knock-down or
63 insertion mutation-based knock-out of *ACR4*, the *Arabidopsis* ortholog of maize CR4, again
64 resulted in epidermis differentiation defects, leading to, for example, abnormal embryo and seed
65 development¹⁷⁻¹⁹. ACR4 localizes to the plasma membrane and to endosomes¹⁷⁻²⁰ and is a

66 catalytically active protein kinase^{18,21-23}. Sequence analysis of four ACR4 homologs in Arabidopsis
67 indicated the presence of a conserved N-terminal β -propeller structure in CRINKLY4
68 ectodomains²¹. Subsequent structure-function studies revealed that kinase null mutations as well as
69 deletion of the putative TNFR domain complemented the *acr4-2* null mutant phenotype^{18,20,24,25}. In
70 contrast, partial deletion of the putative β -propeller domain or mutation of the conserved Cys180 in
71 the β -propeller to tyrosine could not rescue the *acr4-2* phenotype^{20,26}, suggesting an important
72 functional role for the N-terminal segment of the ACR4 ectodomain.

73 β -propeller domains are often involved in protein – ligand or protein – protein interactions²⁷
74 and thus different interaction partners for ACR4 ectodomain have been proposed, following the
75 identification of root specific functions for ACR4^{28,29}. Specifically, the plant peptide hormone
76 CLAVATA3/ESR-RELATED 40 (CLE40) controls expression of the transcription factor
77 WUSCHEL RELATED HOMEOBOX 5 (WOX5) to regulate root stem cell proliferation²⁹. CLE40's
78 signaling capacity depends on the presence of ACR4 and ACR4 has been proposed to act as a direct
79 receptor for CLE40 in the root²⁹⁻³¹. Moreover, ACR4 has been reported to physically interact with
80 the CLAVATA3 (CLV3) / CLE peptide receptor CLAVATA1 (CLV1), forming heteromeric
81 complexes at the plasma-membrane³². In the same study, ACR4 homo-oligomers were observed³².
82 PROTEIN PHOSPHATASE 2A-3 (PP2A-3) and WOX5 have been identified as direct interaction
83 partners for the ACR4 cytoplasmic domain^{33,34}. Here, we uncover the architecture of plant-unique
84 CRINKLY4 RKs by solving crystal structures of ACR4 and *Physcomitrella patens*³⁵ PpCR4.
85

86 **Results**

87 For protein X-ray crystallographic analysis, we produced the ectodomains of ACR4
88 (ACR4^{WD40-CRD}, residues 1 – 423) and PpCR4 (PpCR4^{WD40-CRD}, residues 1 – 405), the isolated β -
89 propeller domain of ACR4 (ACR4^{WD40}, residues 1 – 334) and the kinase domain of ACR4
90 (ACR4^{kinase}, residues 497 – 792) by secreted and cytoplasmic expression in insect cells, respectively.
91 (see Methods) (Fig. 1a). All proteins were purified to homogeneity and the autophosphorylation
92 activity of ACR4^{kinase} could be confirmed (Fig. 1b,c). No crystals were obtained for ACR4^{kinase} and
93 initial crystals of ACR4^{WD40-CRD} and ACR4^{WD40} diffracted poorly. Enzymatic deglycosylation of
94 ACR4^{WD40} yielded a new crystal form diffracting to 1.95 Å resolution. The structure was determined
95 using the multiple anomalous dispersion method on a single crystal derivatized with a platinum
96 compound (see Methods, Supplementary Table 1). Next, enzymatic deglycosylation of PpCR4^{WD40-}
97 ^{CRD} yielded crystals diffracting to 2.7 Å resolution, enabling us to trace the entire CRINKLY4
98 ectodomain (Supplementary Table 1).

99 The N-terminal β -propeller domain of ACR4 and PpCR4 folded into a seven-bladed WD40
100 domain²⁷ (Fig. 1d), as previously speculated²⁰. Each blade is stabilized by a highly conserved
101 disulfide bridge and connected by small loop regions, possibly an evolutionary adaptation to the
102 extracellular environment (Fig. 1d, Supplementary Fig. 1). Cys180, which is found mutated to
103 tyrosine in the *acr4-7* mutant²⁰, forms a disulfide bond in the 4th blade (Fig. 1d). The N- and C-
104 terminal blades are not connected by disulfide bonds (Fig. 1d). The most N-terminal β -strand is
105 buried in the center of the propeller and is highly conserved among all known CRINKLY4
106 receptors³⁶ (Fig. 1d, Supplementary Fig. 1). Several small loops connecting the different blades of
107 the WD40 domain appear partially disordered in our ACR4 and PpCR4 structures (Fig. 1d,e).

108 The C-terminal CRD comprises PpCR4 residues 313-401 and folds into a well defined β -
109 sandwich structure stabilized by six invariant disulfide bridges (Fig. 1e, Supplementary Fig. 1, see
110 below). The WD40 and CRD domains are connected by a short linker region (Fig. 1e). Analysis of
111 crystal lattice arrangements with the program PISA³⁷ and analytical size-exclusion chromatography
112 experiments (Supplementary Fig. 2) together indicate that the ACR4 and PpCR4 ectodomains
113 behave as monomers in solution. All surface exposed cysteines in ACR4 and PpCR4 contribute to
114 disulfide bond formation (Fig. 1d,e; Supplementary Fig. 1). The N-glycosylation pattern differs
115 between ACR4 and PpCR4 (Fig. 1e, Supplementary Fig. 1). Taken together, a compact WD40 and a
116 cysteine-rich domain represent structural fingerprints of monomeric CRINKLY4 ectodomains.

117 Structural homology searches against ACR4^{WD40} using the program DALI³⁸ returned the
118 extracellular WD40 domain of the secreted β -lactamase inhibitor protein II BLIP-II from the soil
119 bacterium *Streptomyces exfoliatus* as top hit (DALI Z-score 23.2, root mean square deviation
120 [r.m.s.d.] is \sim 2.2 Å comparing 192 corresponding C_α atoms) (Supplementary Fig. 3)³⁹. A previously
121 reported homology model of ACR4^{WD40} had been based on the BLIP-II structure²⁰. The UV-B
122 photoreceptor UV-B – RESISTANCE 8 (UVR8) represents the closest structural homolog in plants
123 (Dali Z-score 22.1, r.m.s.d. is \sim 2.4 Å comparing 218 corresponding C_α atoms) (Supplementary
124 Fig.3)⁴⁰. ACR4^{WD40} however lacks the UVR8 tryptophan cage involved in UV-B light sensing^{40,41}
125 and both BLIP-II and UVR8 are devoid of the buried N-terminal strand and the conserved disulfide
126 bridge pattern present in ACR4^{WD40}. Thus, the pore-filling N-terminus and the invariant blade
127 disulfide bonds are unique structural features of extracellular CRINKLY4 WD40 domains.

128 We next studied the interaction of ACR4^{WD40-CRD} with its proposed ligand CLE40²⁹⁻³². As
129 ACR4 has been previously reported to form hetero-oligomers with the LRR-RK CLV1, we sought
130 to include the CLV1 ectodomain in these experiments, but we could not produce well-behaving
131 protein samples of the AtCLV1 ectodomain by secreted expression in insect cells (Supplementary
132 Fig. 4), and consequently could not use the CLV1 ectodomain for biochemical or crystallographic

133 experiments. We thus replaced CLV1 with the LRR ectodomain of the sequence-related CLE
134 peptide receptor BARELY ANY MERISTEM (BAM1) in our *in vitro* binding experiments (Fig. 2a).
135 We found that CLE40 binds the AtBAM1 ectodomain with a dissociation constant (K_d) of $\sim 1 \mu\text{M}$
136 (Fig. 2b) but shows no detectable binding to the ACR4 ectodomain in quantitative grating-coupled
137 interferometry (Fig. 2b) and isothermal titration calorimetry (Fig. 2c) assays. Thus, CLE40 does not
138 represent a direct ligand for the ACR4 ectodomain.

139 Using the previously documented seed retardation phenotype of the *acr4-2* mutant^{18,20} we
140 next carried out genetic complementation analyses using different constructs expressed from the
141 *ACR4* promoter. In agreement with an earlier report²⁰, a construct in which the entire cytoplasmic
142 domain of ACR4 had been deleted could not rescue the seed development phenotypes of *acr4-2*
143 plants (Fig. 3a). Full-length ACR4 lacking kinase activity partially restored seed development in
144 *acr4-2* plants (Fig. 3a). Strikingly, expression of full-length PpCR4, the ectodomain of which shares
145 only 40% sequence identity at the amino-acid level with ACR4^{WD40-CRD}, from the ACR4 promoter
146 could partially complement *acr4-2* phenotypes as well. Together, these experiments reinforce an
147 evolutionary conserved function for CRINKLY4 RKs, which are however not strictly dependent on
148 the protein kinase activity of the receptor.

149 The 2.7 Å crystal structure of the entire ectodomain from PpCR4 enabled us to further
150 characterize the ~ 90 amino-acid CRINKLY4 CRD (Fig. 3b). A structural homology search with
151 DALI³⁸ indeed identified several TNFR domains as top hits, but with very low DALI Z-scores (4.1-
152 2.9). Structural superposition of PpCR4^{CRD} with the previously reported structure of a type I TNF
153 receptor extracellular domain revealed that only a small portion of the CRINKLY4 aligns with
154 canonical TNFR domains (r.m.s.d. is $\sim 1 \text{ \AA}$ comparing 20 corresponding C_α atoms, Fig. 3b). The
155 segment includes a small β-hairpin and two conserved disulfide bridges located at the center of the
156 CRINKLY4 CRD (Fig. 3c). Structural superposition of the eight molecules in the asymmetric unit
157 of our PpCR4^{WD40-CRD} crystal structure (Supplementary Table 1) revealed only subtle movements of
158 the CRD versus the WD40 domain (r.m.s.d. is $\sim 0.3\text{-}0.5 \text{ \AA}$ comparing 360 corresponding C_α atoms,
159 Supplementary Fig. 5). In line with this, we located a small WD40 – CRD domain interface using
160 PISA³⁷ (total buried surface area is $\sim 900 \text{ \AA}^2$). The interface is formed by the C-terminus of the CRD
161 (PpCR4 residues 385-401) that makes mainly hydrophobic interactions with a small groove located
162 between the N- and C-terminal blade of the WD40 domain (Supplementary Fig. 6). Additional
163 contacts originate from a small α-helix in the CRD and several loop regions in PpCR4^{WD40}
164 (Supplementary Fig. 6).

165 Using the now experimentally determined domain boundaries of the ACR4 CRD
166 (Supplementary Figs. 7 and 1), we re-performed complementation assays of the *acr4-2* mutant with

167 a construct in which the entire CRD was omitted (ACR4 ΔCRD). As previously reported^{20,24}, we
168 found that ACR4 ΔCRD can rescue the seed development phenotype of *acr4-2* plants (Fig. 3a).
169 Recently, mutation of the cysteine residues in ACR4^{WD40} and ACR4^{CRD} involved in the formation of
170 disulfide bonds in our structures (Fig. 1, 3b,c) to alanine resulted in a functional receptor for seed
171 development²⁴. We monitored migration of the purified ACR4^{WD40-CRD} ectodomain under oxidizing
172 and strongly reducing conditions in analytical size exclusion chromatography experiments and
173 found that reduction of ACR4^{WD40-CRD} did not induce aggregation of the receptor (Fig. 3d,e).
174 Together, the CRINKLY4 CRD only shares weak structural homology with animal TNFR domains,
175 has a conserved domain interface with the WD40 domain and is dispensable for seed development.
176 The conserved disulfide bonds appear to be involved in structural stabilization. The domain
177 interface between the WD40 domain and the CRD is conserved among CRINKLY4 receptors from
178 different species (Supplementary Figs. 1, 6).

179 While the CRD domain appears to be dispensable for at least some of ACR4's physiological
180 functions, our and previous findings^{20,24} argue for an important role of the structurally unique WD40
181 domain in CRINLKY4 receptors. We located evolutionary conserved, surface exposed residues at
182 the 'back side' of the ACR4 WD40 domain (Fig. 4a, Supplementary Fig. 1), which in our
183 PpCR4^{WD40-CRD} structure is in contact with the CRD (Fig. 1e). We replaced individual residues by
184 alanine or glutamine, respectively and assessed the ability of the resulting mutant proteins to
185 complement the *acr4-2* seed development phenotype (Fig. 4a-c). We analyzed three independent
186 homozygous T3 lines per mutant receptor and found that most mutations behaved similar to wild
187 type (Fig. 4b) and that none of mutants tested displayed the strong loss-of-function phenotype of
188 *acr4-2* plants (Fig. 4b,c). Plants in which either Tyr157 or Asn158/Asn196 were mutated had seed
189 numbers per siliques that were significantly reduced compared to wild type (Fig. 4b). While there
190 was no electron density for a N-glycan at position Asn158 in the ACR4^{WD40} structure (see Methods),
191 the corresponding Asn150 in PpCR4 was found glycosylated (Fig. 1e). ACR4 Asn196 is predicted
192 to be N-glycosylated as well⁴², suggesting that the weak loss-of-function phenotypes observed in
193 our Tyr157/Asn158 and Asn196 point mutants may be caused by an altered N-glycosylation pattern
194 of the receptor (Fig. 4b,c).

195 We next analyzed the molecular surface of the 'front side' of ACR4^{WD40}, which represents
196 another canonical binding surface for peptide and protein ligands in many cytoplasmic or nuclear
197 localized WD40 proteins²⁷. We located a large binding groove in ACR4^{WD40} formed by the WD40
198 domain core and by small surrounding loop regions, which appear similar in our ACR4^{WD40} and
199 PpCR4^{WD40-CRD} WD40 domain structures (r.m.s.d. is ~1.4 Å comparing 246 corresponding C_α atoms,
200 Supplementary Fig. 7). The very low degree of sequence surface conservation in the putative

201 binding groove in apo ACR4^{WD40} renders mutational analysis of the full-length receptor *in planta*
202 difficult (Supplementary Figs. 1, 8). The binding groove is however larger and deeper compared to
203 the VP-peptide binding site in the structurally related WD40 domain of the light-signaling E3
204 ubiquitin ligase CONSTITUTIVELY PHOTOMORPHOGENIC 1 (COP1) (Fig. 4d)⁴³. It may thus
205 provide and interaction platform for high molecular weight ligand.

206

207 Discussion

208 Our crystal structures (Fig. 1d,e) and reverse genetic analyses (Fig. 3a) together reveal an
209 evolutionary conserved domain architecture for plant-unique CRINKLY4 receptor kinases³⁶. The
210 CRINKLY4 WD40 domain differs from known cytoplasmic and extracellular WD40
211 domains^{27,39,40,43}, with its seven blades being stabilized by disulfide bridges and the hydrophobic core
212 of the domain being reinforced by insertion of the protein's N-terminus (Fig. 1d,e). We speculate
213 that these unique structural features represent an adaptation to CRINKLY4 ectodomains being
214 exposed to the plant cell wall environment. Previous²⁰ and our genetic data argue for an important
215 function for the ACR4 WD40 domain in seed development (Fig. 3a). A large groove located on the
216 'front side' of ACR4 may be involved in the binding of a ligand (Fig. 4d). This ligand could be a
217 small molecule, a protein or a peptide, and may be larger than the octameric peptide motifs
218 recognized by COP1 (Fig. 4d). The low degree of sequence conservation of residues contributing to
219 the formation of the binding groove in the WD40 domain (Fig. 4d, Supplementary Fig. 1) and the
220 fact that PpCR4 can functionally replace ACR4's function in Arabidopsis seed development (Fig.
221 3a) together indicate that CRINKLY4 receptors may sense a family of structurally conserved
222 ligands.

223 Our quantitative binding assays reveal that the previously proposed peptide ligand CLE40
224 cannot directly interact with the ACR4 ectodomain (Fig. 2), but we cannot rule out that CLE40
225 binds the CLV1 ectodomain in a signaling complex also containing ACR4^{29,30,32}. The architecture
226 and cellular functions of CLV1 – ACR4 signaling complexes remain to be elucidated, with
227 recombinant expression and purification of the CLV1 ectodomain representing a significant
228 challenge (Supplementary Fig. 4). BAM1 cannot fully replace CLV1 in quantitative biochemical
229 assays, as it binds CLE40 only with moderate affinity (Fig. 2). In contrast, the CLE family member
230 CLE9 binds BAM1 with nanomolar affinity^{44,45}. In solution and in the absence of ligand,
231 CRINKLY4 ectodomains behave as monomers (Fig. 3e, Supplementary Fig. 2). The previously
232 observed ACR4 homo-oligomers³² may thus be generated by ligand-induced oligomerisation of
233 several CRINKLY4 ectodomains and/or be stabilized by interaction of the CRINKLY4 trans-
234 membrane helices, as previously suggested^{46,47}.

235 Analysis of the CRINKLY4 cysteine-rich domain revealed only weak structural homology
236 with animal TNFR domains (Fig. 3b)¹⁴. In line with this, we could not locate proteins with
237 homology to tumor necrosis factors in the *Arabidopsis* or *Physcomitrella patens* genomes^{48,49}. The
238 CRINKLY4 CRD contains six conserved disulfide bridges (Fig. 1e, Supplementary Fig. 1), which
239 in our PpCR4^{WD40-CRD} structure appear to be involved in structural stabilization (Fig. 3b,c). However,
240 CRINKLY4 ectodomains can withstand reducing conditions (Fig. 3e), and thus the putative
241 function of the CRD could indeed be regulated by changes in the cell wall redox environment²⁴.

242 Enzymatic assays of the CRINKLY4 cytoplasmic domains obtained from prokaryotic^{18,21-23}
243 or eukaryotic expression hosts (Fig. 1b,c) clearly identify CRINKLY4s as active protein kinases.
244 Our and previous²⁰ reverse genetic experiments suggest that the ACR4 cytoplasmic domain has to
245 be present for normal seed development in *Arabidopsis*, yet its catalytic activity seems to be
246 dispensable (Fig 1e). Similar observations have been made for CrRLK1L-family receptor kinases⁵⁰⁻
247 ⁵². The mechanistic implications are poorly understood, but the involvement of protein phosphatases
248 in both CR4 and CrRLK1L-mediated signal transduction^{33,53,54} suggests that the cytoplasmic kinases
249 domains of these receptors may act as scaffolding proteins that can become phosphorylated despite
250 not requiring auto- and trans-phosphorylation activity themselves.

251 Genetic interactions between ACR4 and other receptor kinases such as ABNORMAL LEAF
252 SHAPE 2 (ALE2)⁵⁵ the LRR-RKs CLV1^{29,30,32} and GSO1/GSO2^{45,56} have so far not yielded a
253 mechanistic understanding of CRINKLY4's signaling functions. Also, no ligand candidate for
254 ACR4 or for its homologs in *Arabidopsis* has emerged from forward genetic screens²¹. Our
255 identification of a putative ligand binding pocket in ACR4^{WD40} now reinforces the notion that *bona*
256 *fide* ligands for CR4s may exist and that their identification may be achieved using a combination of
257 genetic and biochemical approaches.

258

259 **Material and Methods**

260 **Protein expression and purification**

261 ACR4 coding sequences for the WD40 domain (residues 1 – 334) and its entire ectodomain
262 (residues 1 – 423) were amplified from *A. thaliana* cDNA. PpCR4^{WD40-CRD} (residues 1 – 405),
263 AtCLV1 (residues 25 – 621) and BAM1 (residues 20 – 637) were synthesized by Geneart
264 (Germany) with codon usage optimized for expression in *Trichoplusia ni*. The constructs of ACR4
265 and PpCR4 were cloned in a modified pFastBac vector (Geneva Biotech), containing a TEV
266 (tobacco etch virus protease) cleavable C-terminal StrepII – 9x His tag. ACR4^{WD40-CRD}, CLV1 and
267 BAM1 were also cloned into the vector holding a native signal peptide or the *Drosophila*
268 *melanogaster* BiP secretion signal peptide, respectively, a C-terminal TEV cleavable StrepII – 10x

269 His tag and a non-cleavable Avi-tag^{57,58}. *Trichoplusia ni* (strain Tnao38) cells⁵⁹ were infected with a
270 multiplicity of infection (MOI) of 1 at a density of 2×10^6 cells ml⁻¹ and incubated 26h at 28 °C and
271 48h at 22 °C. The secreted protein was purified from the supernatant by Ni²⁺ affinity
272 chromatography on a HisTrap Excel column (GE healthcare), equilibrated in 50 mM KP_i pH 7.6,
273 250 mM NaCl, 1 mM 2-Mercaptoethanol, followed by StrepII affinity chromatography on a Strep-
274 Tactin XT Superflow high affinity column (IBA), equilibrated in 20 mM Tris pH 8.0, 250 mM
275 NaCl, 1 mM EDTA. The tag was cleaved with His-tagged TEV protease at 4 °C overnight and
276 removed by a second Ni²⁺ affinity chromatography step. Proteins were then further purified by size-
277 exclusion chromatography on either a Superdex 200 increase 10/300 GL, Hi Load 16/600 Superdex
278 200 pg, or a HiLoad 26/600 pg column (GE Healthcare), equilibrated in 20 mM HEPES pH 7.5,
279 150 mM NaCl. For crystallization, ACR4^{WD40} and PpCR4^{WD40-CRD} were dialyzed in 20 mM sodium
280 citrate pH 5.0, 150 mM NaCl and treated with Endoglycosidase H, F1, and F3 to cleave sugar
281 chains. Proteins were then purified by ion exchange chromatography on a HiTrapSP HP column
282 (GE Healthcare), equilibrated in 20 mM Citrate pH 5.0, 25 mM NaCl for ACR4^{WD40} or 20 mM
283 Citrate pH 3.5, 25 mM NaCl for PpCR4^{WD40-CRD}, respectively. Fractions were pooled, concentrated
284 and further purified by size-exclusion chromatography.

285

286 ***In vitro* kinase phosphorylation assay**

287 Coding sequence of ACR4 kinase domain (residues 497 – 792) was amplified from *A.*
288 *thaliana* cDNA and cloned in a modified pFastBac vector harboring a TEV cleavable N-terminal
289 maltose binding protein (MBP) – StrepII – 10x His tag. Point mutation was introduced into the
290 ACR4 (Asp659 → Asn; hereafter ACR4^{D659N}, Supplementary Table 2) coding sequence using the
291 primer extension method for site-directed mutagenesis, rendering the kinase inactive⁶⁰. Insect cells
292 were infected with a MOI of 1 at a density of 2×10^6 cells ml⁻¹ and incubated 26h at 28 °C and 48h
293 at 22 °C. Cells were pelleted by centrifugation at 4,000 x g, 4 °C for 15 min and resuspended in
294 buffer A (20 mM HEPES pH 7.5, 500 mM NaCl, 4 mM MgCl₂ and 2 mM 2-Mercaptoethanol)
295 supplemented with 50 µg ml⁻¹ DNase I, 10 %(v/v) glycerol and 1 tablet of protease inhibitor
296 cocktail (cComplete, Roche), followed by sonication. The cell lysate was centrifuged at 35,000 x g, 4
297 °C for 60 min and the protein was purified from the supernatant by Ni²⁺ affinity chromatography
298 with buffer A, followed by StrepII affinity chromatography. For ACR4^{D659N}, the 10x His – StrepII –
299 MBP tag was cleaved with His-tagged TEV protease at 4 °C overnight and removed by Ni²⁺ affinity
300 chromatography. Proteins were then further purified by size-exclusion chromatography on a
301 Superdex 200 increase 10/300 GL column equilibrated in 20 mM Tris-HCl pH 8, 250 mM NaCl, 4
302 mM MgCl₂ and 0.5 mM TCEP. Monomeric peak fractions were collected and concentrated for

303 analyses. For *in vitro* kinase assays, 2 µg of MBP-ACR4 and 1 µg of ACR4^{D659N} were used in a
304 reaction volume of 20 µl. The reactions were started by addition of 5 µCi [γ -³²P]-ATP (Perkin-
305 Elmer, Waltham, MA), incubated at room temperature for 45 min and terminated by the addition of
306 6x SDS loading dye, immediately followed by heating the samples at 95 °C. Proteins were
307 separated by SDS-PAGE in 4 – 15 % gradient gels (TGX, Biorad) and ³²P-derived signals were
308 visualized by exposing the gel to an X-ray film (SuperRX, Fujifilm).

309

310 **Crystallization and data collection**

311 Crystals of the deglycosylated ACR4^{WD40} and PpCR4^{WD40-CRD} developed at room temperature
312 in hanging drops composed of 1 µl protein solution (ACR4^{WD40}, 20 mg/ml; PpCR4^{WD40-CRD}, 16
313 mg/ml) 1 µl of crystallization buffer (16 % PEG 6,000, 0.01 M tri-sodium citrate pH 5.0 for
314 ACR4^{WD40}, 15 % PEG 4,000, 0.2 M imidazole malate pH 7.0 in the case of PpCR4^{WD40-CRD})
315 suspended above 1.0 ml of the latter as reservoir solution and using microseeding protocols.
316 Crystals were cryo-protected by serial transfer into crystallization buffer supplemented with 20 %
317 (v/v) ethylene glycol and snap-frozen in liquid nitrogen. For heavy-atom derivatization, crystals of
318 ACR4^{WD40} were transferred in the crystallization buffer containing 2 mM K₂[Pt(CNS)₆] and
319 incubated for 2.5h. Crystals were cryo-protected by serial transfer into crystallization buffer
320 supplemented with 20 % (v/v) glycerol and cryo-cooled in liquid nitrogen. Platinum multi-
321 wavelength anomalous diffraction (MAD) data were collected to 3.2 Å resolution was collected at
322 beam-line PXIII at the Swiss Light Source (SLS), Villigen, CH. A native data for ACR4^{WD40} and
323 PpCR4^{WD40-CRD} were recorded at a resolution of 1.95 Å and 2.70 Å, respectively (Supplementary
324 Table 1). Data processing and scaling were done with XDS and XSCALE⁶¹.

325

326 **Structure solution and refinement**

327 Nine consistent Pt sites were located in three wavelength MAD data using the program
328 SHELXD⁶² followed by site refinement and phasing in SHARP⁶³. The resulting heavy atom sites
329 and starting phases (FOM was 0.35 to 3.2 Å resolution) were input into phenix.autobuild⁶⁴ for non-
330 crystallographic symmetry (NCS) averaging, phase extension, density modification (FOM was 0.75
331 to 1.95 Å resolution) and iterative model building. The refined (Refmac5⁶⁵) model comprises four
332 ACR4^{WD40} molecules in the asymmetric unit with an associated solvent content of 0.42. The space
333 group *P* 2₁ with a β angle of 90.1° was validated using the programs POINTLESS⁶⁶ and
334 ZANUDA⁶⁷. The structure of PpCR4^{WD40-CRD} was solved using the molecular replacement method
335 using an ACR4^{WD40} monomer as search model in calculations with the program PHASER⁶⁸. The
336 solution comprises eight PpCR4^{WD40-CRD} molecules in the asymmetric unit. The structure was

337 completed in alternating cycles of manual model building in COOT⁶⁹ and restrained NCS
338 refinement in phenix.refine⁷⁰. Ile156 represents a Ramachandran plot outlier in each chain, but is
339 well defined by electron density. Structural diagram were prepared in Pymol
340 (<https://sourceforge.net/projects/pymol/>) and ChimeraX⁷¹.

341

342 **Biotinylation of proteins**

343 The respective proteins (20 – 100 μ M) were biotinylated with biotin ligase BirA⁵⁸ (2 μ M)
344 for 1h at 25 °C, in a volume of 200 μ l; 25 mM Tris pH 8, 150 mM NaCl, 5 mM MgCl₂, 2 mM 2-
345 Mercaptoethanol, 0.15 mM Biotin, 2 mM ATP, followed by size-exclusion chromatography to
346 purify the biotinylated proteins.

347

348 **Grating – coupled interferometry**

349 GCI experiments were performed with the Creoptix WAVE system (Creoptix AG,
350 Switzerland), using 4PCP WAVE chips (thin quasiplanar polycarboxylate surface; Creoptix,
351 Switzerland). Chips were conditioned with borate buffer (100 mM sodium borate pH 9.0, 1 M
352 NaCl; Xantec, Germany) and activated with 1:1 mix of 400 mM *N*-(3-dimethylaminopropyl)-*N*'-
353 ethylcarbodiimide hydrochloride and 100 mM *N*-hydroxysuccinimide (Xantec, Germany) for 7 min.
354 Streptavidin (50 μ g ml⁻¹; Sigma, Germany) in 10 mM sodium acetate pH 5.0 (Sigma, Germany) was
355 immobilized on the chip surfaces and passivated with 0.5 % BSA (Roche, Switzerland) in 10 mM
356 sodium acetate pH 5.0, followed by final quenching with 1M ethanolamine pH 8.0 (Xantec,
357 Germany) for 7 min. Biotinylated ligands (20 – 50 μ g ml⁻¹) was captured by streptavidin
358 immobilized on the chip surface. All kinetic analyses were performed at 25°C with a 1:2 dilution
359 series from 10 μ M of CLE40 peptides in 20 mM citrate pH 5.0, 250 mM NaCl, 0.01 % Tween 20.
360 Blank injections were used for double referencing and a dimethylsulfoxide (DMSO) calibration
361 curve for bulk correction. Analysis and correction of the obtained data was performed using the
362 Creoptix WAVE control software (correction applied: X and Y offset; DMSO calibration; double
363 referencing). Mass transport binding models with bulk correction were used. Experiments were
364 performed in triplicates.

365

366 **Isothermal titration calorimetry**

367 All ITC experiments were performed on a MicroCal PEAQ-ITC (Malvern Panalytical) with
368 a 200 μ l sample cell and a 40 μ l injection syringe at 25 °C. Proteins were dialyzed into ITC buffer
369 (20 mM sodium citrate pH 5.0, 250 mM NaCl) prior to all experiments. The CLE40 peptide
370 (RQV[Hyp]TGSDPLHH) was synthesized (Peptide Specialty Labs GmbH) and dissolved directly

371 in buffer. The dissolved peptide concentration was measured by right-angle light scattering
372 (OMNISEC RESOLVE / REVEAL combined system, Malvern Panalytical). The protein
373 concentrations were calculated based on their absorbance at 280 nm and their corresponding molar
374 extinction coefficient. A typical experiment consisted of injecting 19 injections of 2 μ l of 1000 μ M
375 CLE40 into the cell containing 100 μ M ACR4. Experiments were performed in triplicates.
376

377 **Plant materials and generation of transgenic lines**

378 *Arabidopsis thaliana* ecotype Columbia (Col-0) and SAIL_240_B04 (*acr4-2*¹⁸) were used
379 for all experiments. *ACR4* gene (residues 1 – 895) and *ACR4* promoter region (*pACR4*, 1847 bp
380 upstream from ATG) were amplified from *A. thaliana* genomic DNA. *PpCR4* (residues 1 – 893)
381 gene with *Physcomitrella patens* CDS was synthesized (Geneart, Germany). The coding sequences
382 were cloned in a pDONR 221 Gateway vector (Invitrogen) and *pACR4* sequence was cloned in a
383 pDONR P4-P1R Gateway vector (Invitrogen). *ACR4* variants carrying deletion or point mutations
384 were generated using the primer extension method. pDONR P2R-P3 Gateway vector harboring
385 mCitrine or 6x HA tag were used to attach C-terminal tag. Expression constructs were generated
386 with LR Gateway Cloning (Invitrogen) in pH7m34GW⁷²; *pACR4::ACR4* (residues 1 – 895)-
387 mCitrine, *pACR4::ACR4_ΔCyto* (residues 1 – 492)-mCitrine, *pACR4::PpCR4* (residues 1 – 893)-
388 mCitrine, *pACR4::ACR4_ΔCRD* (residues 1 – 895 with deletion 335 – 423)-mCitrine,
389 *pACR4::ACR4_K540R-HA*, *pACR4::ACR4_D84A-mCitrine*, *pACR4::ACR4_F105A-mCitrine*,
390 *pACR4::ACR4_D127A-mCitrine*, *pACR4::ACR4_Y157A-mCitrine*, *pACR4::ACR4_N158A-*
391 *mCitrine*, *pACR4::ACR4_Y157A*, *N158A-mCitrine*, *pACR4::ACR4_Y218A-mCitrine*,
392 *pACR4::ACR4_N158Q*, *N196Q-HA*. They were transformed in *acr4-2* background by floral
393 dipping method⁷³ with *Agrobacterium tumefaciens* strain GV3101 (Supplementary Table 3).
394

395 **Seed counting and statistical analysis**

396 Plants were germinated on 0.5 MS (Murashige and Skoog) agar plates after 3 days in dark at
397 4°C. Seedling were transferred to soil and grown at 22°C, under long days (16 h light / 8 h dark) for
398 6 weeks. A top opened flower was defined as position 1 and a siliques at position 12 was collected
399 for analyses in a blind manner. 10 siliques were sampled for independent lines as biological
400 replicates and seeds were counted under a stereo microscope. The simultaneous comparisons of the
401 different transgenic lines vs wild type were performed using the Dunnett procedure⁷⁴ for the primary
402 endpoint number seeds per siliques using the count transformation model⁷⁵. The Comprehensive R
403 Archive Network packages multcomp⁷⁶ and cotram⁷⁵ were used in R, version 3.6.3.
404

405 **Data availability**

406 Data supporting the findings of this manuscript are available from the corresponding authors
407 upon reasonable request. A reporting summary for this article is available as a Supplementary
408 Information file. Coordinates and structure factors have been deposited in the Protein Data Bank
409 (PDB) with accession codes 7A0J (ACR4^{WD40}) and 7A0K (PpCR4^{WD40-CRD}).

410

411 **Acknowledgments**

412 We thank K. Lau for help with crystallographic data collection and U. Hohmann, D. Couto
413 and J. Santiago for providing feedback on the manuscript. This work was supported by grants
414 31003A_176237 and 31CP30_180213 from the Swiss National Science Foundation (to MH), by a
415 Howard Hughes Medical Institute (HHMI) International Research Scholar Award (to MH) and by a
416 Human Frontier Science Program (HFSP) postdoctoral fellowship (to SO).

417

418 **Author contributions**

419 MH and SO designed the study, SO performed all biochemical and genetic experiments, SO
420 and MH phased and refined the structures, LAH performed the statistical analysis and SO and MH
421 wrote the manuscript.

422

423 **Conflict of interest**

424 The authors declare no conflict of interest.

425

426 **Figure legends**

427 **Figure 1. CRINKLY 4 receptor kinases harbor structurally unique β-propeller and cysteine-
428 rich domains.**

429 **a**, ACR4 domain scheme: SP, signal peptide; WD40, WD40 domain; CRD, cysteine-rich domain;
430 TM, transmembrane helix; JM, juxtamembrane region; CT, C-terminal tail. **b**, SDS-PAGE analysis
431 of purified CRINKLY4 proteins expressed in insect cells. **c**, Autoradiography *in vitro* kinase assay
432 of the wild-type ACR4 kinase domain fused to maltose-binding protein (MBP), and of the unfused
433 kinase domain carrying a point mutation (Asp659 → Asn) in the active site. The coomassie-stained
434 gel loading control is shown in b (lanes on the right of the dotted line). **d**, Ribbon diagrams of
435 ACR4^{WD40} in two orientations and colored from N- (yellow) to C-terminus (green). Disulfide bonds
436 are shown in bonds representation and highlighted by yellow circles. **e**, Structure of PpCR4^{WD40-CRD}
437 shown in two different orientations and colored in blue (WD40 domain) and yellow (CRD),

438 respectively. The N-glycans visible in the electron density map are depicted in bonds representation
439 (in gray).c
440

441 **Figure 2. The ACR4 ectodomain does not bind the peptide hormone CLE40 *in vitro*.**

442 **a**, SDS-PAGE analysis of the biotinylated ACR4^{WD40-CRD} and AtBAM1^{LRR} ectodomains used for
443 binding experiments. **b**, Quantitative grating-coupled interferometry (GCI) binding assay of a
444 synthetic CLE40 peptide versus ACR4^{WD-CRD} and BAM1^{LRR}. Shown are sensorgrams with raw data
445 in red and their respective fits in black. Table summaries of kinetic parameters are shown alongside
446 (D_c, density of captured protein; k_t, mass transport coefficient; k_{on}, association rate constant; k_{off},
447 dissociation rate constant; K_d, dissociation constant; n.d., no detectable binding, n=3). **c**, Isothermal
448 titration calorimetry (ITC) experiment of ACR4^{WD-CRD} versus CLE40. No binding was detected in
449 this assay (n=3).
450

451 **Figure 3. CRINKLY4 ectodomains harbor an evolutionary conserved function.**

452 **a**, Reverse genetic rescue experiments of the seed development phenotype of *acr4-2*. Left panel:
453 Seed development phenotypes of wild type, *acr4-2* and a complemented line. Right panel: Ten
454 siliques per transgenic line from three independent homozygous T3 lines were pooled and plotted as
455 beeswarm plots with the bold line representing mean, whiskers indicating the standard deviation,
456 and circles depicting the raw data. Seed counts per siliques significantly different from wild type
457 were determined by simultaneous comparisons of several mutants against wild type using the
458 Dunnett procedure (indicated by an asterisk). **b**, Ribbon diagram overview of PpCR4^{WD40-CRD} (colors
459 as in Fig. 1) and close-up view of the CRD superimposed to a type I TNF receptor ectodomain
460 (PDB-ID 1NCF⁷⁷; in gray). The six invariant disulfide bridges of CRINKLY4 CRDs are shown in
461 green, the disulfide bonds in TNFR are shown in gray (in bonds representation). **c**, Superposition of
462 the structurally homologous PpCR4^{CRD} (in yellow) and TNFR (in gray) core segments (r.m.s.d. is ~1
463 Å comparing 20 corresponding C_α atoms). **d**, Analytical size-exclusion chromatography of
464 ACR4^{WD40-CRD} in the pre- or absence of Tris(2-carboxyethyl)phosphine (TCEP). Void (V₀), total (V_t),
465 and elution volumes for molecular-mass standards (Al, Aldolase, 158 kDa; Co, Conalbumin, 75
466 kDa; Ov, Ovalbumin, 44 kDa; CA, Carbonic Anhydrase, 29 kDa; R, Ribonuclease A, 13.7 kDa; Ap,
467 Aprotinin; 6.5 kDa) are indicated. **e**, SDS-PAGE analysis of fractions shown in d.
468

469 **Figure 4. The CRINKLY4 WD40 domain contains a putative ligand binding groove.**

470 **a**, Ribbon diagram of ACR4^{WD40} (in blue) with surface exposed conserved residues shown in bonds
471 representation (in orange) at the exposed surface. Blade numbers are indicated. **b**, Effect on surface

472 point-mutations on ACR4-mediated seed production. Ten siliques per transgenic line from three
473 independent homozygous T3 complementation lines were pooled and plotted as beeswarm plots
474 with the bold line representing mean, whiskers indicating the standard deviation, and circles
475 depicting the raw data. The plots for wild type, *acr4-2* and *ACR4* were generated from same data
476 sets shown in Fig. 3a. Seed counts per siliques significantly different from wild type were
477 determined by simultaneous comparisons of several mutants against wild type using the Dunnett
478 procedure (indicated by an asterisk). **c**, Molecular surface of the *ACR4*^{WD40} β -propeller domain
479 ‘back side’ (in light blue). The positions of the mutated residues are highlighted in orange. **d**,
480 Comparison of the ‘front sides’ of the structurally related WD40 domains of COP1 (PDB-ID
481 6QTO⁴³ left panel) and ACR4 (right panel, r.m.s.d is ~3.5 comparing 205 corresponding C_α atoms).
482 The COP1 VP-peptide ligand derived from the transcription factor HY5 is shown in yellow. Note
483 the large and deep putative binding groove in the corresponding surface area in *ACR4*^{WD40}.
484

485 **Supplementary Figure 1. Structure-based multiple sequence alignment of CRINKLY4**
486 **receptor ectodomains from different species.**

487 Structure based T-COFFEE⁷⁸ sequence alignment and including a secondary structure assignment
488 calculated with DSSP⁷⁹ (WD40 domain in blue, CRD in yellow). Invariant cysteine residues
489 contributing to disulfide bonds in the WD40 domain or CRD domain are highlighted in yellow and
490 green, respectively. Residues analyzed with point mutations in this study are shown in orange.
491 Conserved residues in the WD40 – CRD domain interface are depicted in gray. Asterisks denote the
492 location of experimentally confirmed N-glycosylation sites. Red arrows represent domain
493 boundaries for the Δ TNFR/CRD deletion constructs in previous reports: (1)²⁴, (2)²⁰. ACR4
494 (*Arabidopsis thaliana*) UNIPROT-ID (<http://uniprot.org>) Q9LX29; PpCR4 (*Physcomitrella patens*)
495 A9RKG8; ZmCR4 (*Zea mays*) O24585; OsCR4 (*Oryza sativa*) Q75J39; SmCR4 (*Selaginella*
496 *moellendorffii*) D8T625. Note that the annotated SmCR4 sequence may be incomplete.
497

498 **Supplementary Figure 2. CRINKLY4 receptor ectodomains behave as monomers in solution.**

499 Analytical size-exclusion chromatography of the *ACR4*^{WD40-CRD}, *ACR4*^{WD40} and PpCR4^{WD40-CRD} in the
500 presence or absence of enzymatic deglycosylation. The void volume (V₀), the total column volume
501 (V_t), and the elution volumes for molecular-mass standards (Al, Aldolase, 158 kDa; Co,
502 Conalbumin, 75 kDa; Ov, Ovalbumin, 44 kDa; CA, Carbonic Anhydrase, 29 kDa; R, Ribonuclease
503 A, 13.7 kDa; Ap, Aprotinin; 6.5 kDa) are indicated.
504

505 **Supplementary Figure 3. ACR4^{WD40} shares structural features with known WD40 domains.**

506 Structural superposition of ACR4^{WD40} (blue ribbon diagram) with **a**, the secreted β -lactamase
507 inhibitor protein II BLIP-II (PDB-ID 1JTD³⁹, in yellow) from the bacterium *Streptomyces exfoliatus*
508 (r.m.s.d. is \sim 2.2 Å comparing 192 corresponding C_α atoms), and **b**, with the WD40 domain of the
509 UV-B photoreceptor UVR8 (PDB-ID 4D9S⁴⁰, r.m.s.d. is \sim 2.4 Å comparing 218 corresponding C_α
510 atoms). Note that SeBLIP-II and UVR8 shares the blade number and overall architecture with
511 ACR4^{WD40}, but lack the buried N-terminal strand and the conserved disulfide bonds stabilizing each
512 blade.

513

514 **Supplementary Figure 4. Expression and purification attempts of the AtCLV1 LRR**
515 **ectodomain.**

516 Shown are immunoblot analyses monitoring the secreted expression of the AtCLV1 ectodomain
517 (see Methods) with an anti-His antibody (left panels, Day, days post infection, MOI, multiplicity of
518 infection; SN, supernatant; P, pellet). Right panel: Preparative size-exclusion chromatography of the
519 purified AtCLV1 ectodomain reveals the presence of large aggregates. The void (V₀), total (V_t), and
520 elution volumes for molecular-mass standards (Al, Aldolase, 158 kDa; Co, Conalbumin, 75 kDa;
521 Ov, Ovalbumin, 44 kDa; CA, Carbonic Anhydrase, 29 kDa; R, Ribonuclease A, 13.7 kDa; Ap,
522 Aprotinin; 6.5 kDa) are indicated.

523

524 **Supplementary Figure 5. Only small WD40 - CRD inter-domain movements can be observed**
525 **in the PpCR4 crystal structure.**

526 Structural superposition of the eight molecules located in the asymmetric unit of the PpCR4^{WD40-CRD}
527 crystal structure (r.m.s.d. is \sim 0.3-0.5 Å comparing 360 corresponding C_α atoms). Individual
528 molecules are shown in different colors as C_α traces.

529

530 **Supplementary Figure 6. Overview of the WD40 – CRD domain interface in the PpCRD^{WD40-}**
531 **CRD structure.**

532 Shown is a ribbon diagram of the PpCR4 ectodomain (colored according to Fig. 1e) with selected
533 interface residues shown in bonds representation. Hydrogen bonds and salt bridges are indicated by
534 dotted lines.

535

536 **Supplementary Figure 7. Structural visualization of the TNFR/CRD domain boundaries used**
537 **in this and in previous studies.**

538 Ribbon diagram of PpCR4^{WD40-CRD} with the WD40 domain shown in blue and the experimentally
539 determined CRD domain boundaries shown in yellow (left panel). The previously used TNFR

540 domain boundaries^{20,24} derived from sequence analysis (in orange) omit the most N-terminal β -
541 strand in the CRD (in blue, indicated by a black arrow).

542

543 **Supplementary Figure 8. Structurally conserved loop regions contribute to the formation of a**
544 **putative ligand binding groove in CRINKLY4 WD40 domains.**

545 **a**, Structural superposition of the isolated WD40 domain from ACR4 (blue) and PpCR4 (light gray,
546 r.m.s.d. is is ~ 1.4 Å comparing 246 corresponding C_α atoms reveals the loop regions contributing to
547 the formation of a putative ligand binding groove to adopt similar orientations in both structures. **b**,
548 A temperature (B-) factor plot of PpCR4^{WD40-CRD} (molecule chain A) reveals little structural
549 flexibility for the secondary structure elements forming part of the putative binding groove, while
550 the partially disordered loops connecting the blades of the β -propeller and the loops connecting the
551 CRD appear mobile in the PpCR4^{WD40-CRD} crystal structure.

552 **Supplementary Table 1. Crystallographic data collection and refinement statistics.**

PDB-ID	ACR4 ^{WD40} 7A0J	PpCR4 ^{WD40-CRD} 7A0K
Data collection		
Space group	<i>P</i> 2 ₁	<i>P</i> 2 ₁
Cell dimensions		
<i>a, b, c</i> (Å)	75.0, 88.0, 88.6, 90, 90.1, 90	88.6, 184.0, 98.2
α, β, γ (°)	90, 90.1, 90	90, 96.1, 90
Resolution (Å)	48.05 – 1.95 (2.07 – 1.95)	45.87 – 2.70 (2.86 – 2.70)
$R_{\text{meas}}^{\#}$	0.125 (1.94)	0.151 (1.89)
CC(1/2) [#]	1.0 (0.4)	1.0 (0.46)
$I/\sigma I^{\#}$	8.75 (0.91)	12.01 (0.98)
Completeness (%) [#]	99.7 (98.3)	99.9 (99.7)
Redundancy [#]	6.8 (6.6)	7.0 (6.6)
Wilson B-factor [#]	40.2	71.5
Refinement		
Resolution (Å)	48.05 – 1.95	45.87 – 2.70
No. reflections	79,774	85,621
$R_{\text{work}}/ R_{\text{free}}^{\$}$	0.22 (0.24)	0.22 (0.25)
No. atoms		
protein	7,980	20,414
carbohydrate/buffer	106	524
solvent	270	134
Res. B-factors ^{\$}		
protein	53.7	90.8
carbohydrate/buffer	61.6	97.6
solvent	48.4	66.1
R.m.s deviations ^{\$}		
bond lengths (Å)	0.0135	0.0027
bond angles (°)	1.64	0.60
Ramachandran plot ^{\$} :		
most favored regions (%)	97.0	96.1
outliers (%)	0	0.2
MolProbity score ^{\$}	1.06	1.27

553 ^{*}as defined in XDS⁶¹

554 ⁺as defined Refmac5⁶⁵ or phenix.refine⁷⁰

555 ^{\$}as defined in Molprobity⁸⁰

556 **Supplementary Table 2. Primers used in this study**

Primer Name	Sequence	Description
ACR4prom_B4-F	GGGGACAACTTGTATAGAAAAGTTGACGAGATAGTCAAGAA ATGGCCTTC	cloning of ACR4 promoter region
ACR4prom_B1r-R	GGGGACTGCTTTTGACAAACTGCTTTCAAAGTCAAC ACACACG	cloning of ACR4 promoter region
ACR4cds_B1-F	GGGGACAAGTTGTACAAAAAAGCAGGCTGAATGAGAATGTT CGAAACGAGAG	cloning of ACR4 coding sequence
ACR4cds_B2r-R	GGGGACCACTTGTACAAGAAAGCTGGTAGAAATTATGATG CAAGAACAAAGC	cloning of ACR4 coding sequence
ACR4delK_B2rR	GGGGACCACTTGTACAAGAAAGCTGGTATTGCAGCTCATC AAGATC	Δcyto construct for transgenic plant
ACR4_K540R_For	GCAGTGAGAAGAGCGATAATGTCATCAGACAAACAGAAG	site directed mutagenesis for transgenic plant
ACR4_K540R_Rev	CGCTCTTCTCACTGCAACAGTGGTCCATCTCTCAG	site directed mutagenesis for transgenic plant
ACR4_delTNFR_Fw	CCTGCTCTATCCCTAAGTTGGTCACTGCAGCTAC	ΔCRD construct for transgenic plant
ACR4_delTNFR_Rv	CAGTGACCAAAACTTAGGGATAGAAGCAGGGAAACC	ΔCRD construct for transgenic plant
ACR4_D84A_F	GGGTGGAGCTGGTTATGTGTGGC	site directed mutagenesis for transgenic plant
ACR4_D84A_R	ATAAACCCAGCTCCACCGTTAACCG	site directed mutagenesis for transgenic plant
ACR4_F105A_F	CAGTGCAGCTATTCAAATGGGAGTTCCTC	site directed mutagenesis for transgenic plant
ACR4_F105A_R	ATTTGAATAGCTGCACTGTTCCCCAAC	site directed mutagenesis for transgenic plant
ACR4_D127A_F	TGCTGGTGCTTACCATCTTGTGGTTGAG	site directed mutagenesis for transgenic plant
ACR4_D127A_R	AGATGGTAAGCACCAGCACTAACTTCTAAATAC	site directed mutagenesis for transgenic plant
ACR4_Y157A_F	TTGGGGTGCTAATATGACAAGAAACTTGTCTTG	site directed mutagenesis for transgenic plant
ACR4_Y157A_R	GTCATATTAGCACCCAAACAATCAACAAG	site directed mutagenesis for transgenic plant
ACR4_N158A_F	GGGTTACGCTATGACAAGAAACTTGTCTTG	site directed mutagenesis for transgenic plant
ACR4_N158A_R	CTTGTCAAGCGTAACCCAAACAATCAAC	site directed mutagenesis for transgenic plant
ACR4_Y157,N158A_F	TTGGGGTGCTATGACAAGAAACTTGTCTTG	site directed mutagenesis for transgenic plant
ACR4_Y157,N158A_R	CTTGTCAAGCAGCACCCAAACAATCAACAAG	site directed mutagenesis for transgenic plant
ACR4_Y218A_F	TGGTGGAGCTATGTTGTGGCATTCTTG	site directed mutagenesis for transgenic plant
ACR4_Y218A_R	ACAAACATGAGCTCCACCAGCTGCAATTTC	site directed mutagenesis for transgenic plant
ACR4_N158Q_For	GGTTACCAAGATGACAAGAAACTTGTCTTGATAAGCAG	site directed mutagenesis for transgenic plant
ACR4_N158Q_Rev	TGTCATCTGTAACCCAAACAATCAACAAG	site directed mutagenesis for transgenic plant
ACR4_N196Q_For	GATGAGCAGAGTAGTCAAGTAATCAGTTAACCCAAAG	site directed mutagenesis for transgenic plant
ACR4_N196Q_Rev	ACTACTCTGCTCATCTCCCAACAGAAAACCGAC	site directed mutagenesis for transgenic plant
ACR4_pBB2_ins_f	TTATTCATACCGTCCCACCATGGCGCGGATGAGAATGTTG AAACGAGAG	protein expression in insect cell
334-pBB2_Rv	CCCTGGAAGTACAGGTTCTCGAGTTAGGGATAGAAGCAGGG AAAC	protein expression in insect cell
ACR4_pBB2_423r	CATGCAGAGCCCTGGAAGTACAGGTTCTCGAGTCCTTTTCCT TGCCTCCAC	protein expression in insect cell
ACR4_423_Avi_Rv	AGCCTCGAAGATGTCGTTCAGACCCCTGAGTCCTTTCTTG CCTCCACTGGTAGCC	protein expression in insect cell
ACR4_497-F_Nco1	CGGCCATGGCTAGAGTTTCACTTATGAGGAACCTG	protein expression in insect cell
ACR4_792-R_Not1	TTAGCGGCCGCTTATTATAGCTGTGCAAGCGCTCG	protein expression in insect cell
PpCR4_pBB2_Fw	ATACCGTCCCACCATGGCGCGGGAGCTCATGCCTGTACTCG TGC	protein expression in insect cell
PpCR4_P405_Rv	TCGAAGATGTCGTTCAGACCCCTGAGTGGAGCCTTGAAGGG TTATAAC	protein expression in insect cell
CLV1co_T25_Fw	TGTTGGCCTCTCGCTCGGGCTACCATGGGATACACCGACATG GAGGTGC	protein expression in insect cell

CLV1co_P621_Rv	AGCCTCGAAGATGTCGTTCAGACCCTCGAGAGGGCAGGACA CACGG	protein expression in insect cell
BAM1_BiP_F	CTTTGTTGGCCTCTCGCTGGGGCTACCATGGGACGACCAATC TCCGAG	protein expression in insect cell
BAM1_Avi_R	AGCCTCGAAGATGTCGTTCAGACCCTCGAGTGTATAAGGTCC TITACTATGACTC	protein expression in insect cell
ACR4_D659N_For	GTAGCTAACTTGGTCTCTCCTTACTTGGTCCTGTCG	site directed mutagenesis for kinase-dead recombinant protein
ACR4_D659N_Rev	GACCAAAGTTAGCTACTCGAGCATTGTGTTCTTCATC	site directed mutagenesis for kinase-dead recombinant protein

557 F, For, Fw: Forward; R, Rev, Rv: Reverse

558

559 **Supplementary Table 3. Transgenic lines generated in this study**

Name	residues (amino acids)	Tag	Resistance	Genetic background
ACR4	1 – 895	mCitrine	Hygromycin	<i>acr4-2</i>
ACR4 Δcyto	1 – 492	mCitrine	Hygromycin	<i>acr4-2</i>
ACR4 kinase dead	1 – 895 (K540R)	6x HA	Hygromycin	<i>acr4-2</i>
ACR4 ΔCRD	1 – 895 with deletion 335 – 423	mCitrine	Hygromycin	<i>acr4-2</i>
PpCR4	1 – 893	mCitrine	Hygromycin	<i>acr4-2</i>
ACR4 D84A	1 – 895 (D84A)	mCitrine	Hygromycin	<i>acr4-2</i>
ACR4 F105A	1 – 895 (F105A)	mCitrine	Hygromycin	<i>acr4-2</i>
ACR4 D127A	1 – 895 (D127A)	mCitrine	Hygromycin	<i>acr4-2</i>
ACR4 Y157A	1 – 895 (Y157A)	mCitrine	Hygromycin	<i>acr4-2</i>
ACR4 N158A	1 – 895 (N158A)	mCitrine	Hygromycin	<i>acr4-2</i>
ACR4 Y157A, N158A	1 – 895 (Y157A/N158A)	mCitrine	Hygromycin	<i>acr4-2</i>
ACR4 N158Q, N196Q	1 – 895 (N158Q/N196Q)	6x HA	Hygromycin	<i>acr4-2</i>
ACR4 Y218A	1 – 895 (Y218A)	mCitrine	Hygromycin	<i>acr4-2</i>

560

561 References

1. Shiu, S. H. & Bleecker, A. B. Receptor-like kinases from *Arabidopsis* form a monophyletic gene family related to animal receptor kinases. *Proc. Natl. Acad. Sci. U. S. A.* **98**, 10763–10768 (2001).
2. Hohmann, U., Lau, K. & Hothorn, M. The Structural Basis of Ligand Perception and Signal Activation by Receptor Kinases. *Annu. Rev. Plant Biol.* **68**, 109–137 (2017).
3. Bozsoki, Z. *et al.* Receptor-mediated chitin perception in legume roots is functionally separable from Nod factor perception. *Proc. Natl. Acad. Sci. U. S. A.* **114**, E8118–E8127 (2017).
4. Liu, T. *et al.* Chitin-Induced Dimerization Activates a Plant Immune Receptor. *Science* **336**, 1160–1164 (2012).
5. Liu, S. *et al.* Molecular Mechanism for Fungal Cell Wall Recognition by Rice Chitin Receptor OsCEBiP. *Structure* **24**, 1192–1200 (2016).
6. Ma, R. *et al.* Structural basis for specific self-incompatibility response in *Brassica*. *Cell Res.* **26**, 1320–1329 (2016).
7. Moussu, S. & Santiago, J. Structural biology of cell surface receptor-ligand interactions. *Curr. Opin. Plant Biol.* **52**, 38–45 (2019).
8. Vaattovaara, A. *et al.* Mechanistic insights into the evolution of DUF26-containing proteins in land plants. *Commun. Biol.* **2**, 56 (2019).
9. Moussu, S., Augustin, S., Roman, A. O., Broyart, C. & Santiago, J. Crystal structures of two tandem malectin-like receptor kinases involved in plant reproduction. *Acta Crystallogr. Sect. Struct. Biol.* **74**, 671–680 (2018).
10. Xiao, Y. *et al.* Mechanisms of RALF peptide perception by a heterotypic receptor complex. *Nature* **572**, 270–274 (2019).
11. Moussu, S. *et al.* Structural basis for recognition of RALF peptides by LRX proteins during pollen tube growth. *Proc. Natl. Acad. Sci. U. S. A.* **117**, 7494–7503 (2020).
12. Becraft, P. W., Stinard, P. S. & McCarty, D. R. CRINKLY4: A TNFR-like receptor kinase involved in maize epidermal differentiation. *Science* **273**, 1406–1409 (1996).
13. Jin, P., Guo, T. & Becraft, P. W. The maize CR4 receptor-like kinase mediates a growth factor-like differentiation response. *Genesis* **27**, 104–116 (2000).

14. Banner, D. W. *et al.* Crystal structure of the soluble human 55 kd TNF receptor-human TNF beta complex: implications for TNF receptor activation. *Cell* **73**, 431–445 (1993).
15. Sprang, S. R. The divergent receptors for TNF. *Trends Biochem. Sci.* **15**, 366–368 (1990).
16. Becraft, P. W., Kang, S. H. & Suh, S. G. The maize CRINKLY4 receptor kinase controls a cell-autonomous differentiation response. *Plant Physiol.* **127**, 486–496 (2001).
17. Tanaka, H. *et al.* ACR4, a putative receptor kinase gene of *Arabidopsis thaliana*, that is expressed in the outer cell layers of embryos and plants, is involved in proper embryogenesis. *Plant Cell Physiol.* **43**, 419–428 (2002).
18. Gifford, M. L., Dean, S. & Ingram, G. C. The *Arabidopsis* ACR4 gene plays a role in cell layer organisation during ovule integument and sepal margin development. *Development* **130**, 4249–4258 (2003).
19. Watanabe, M., Tanaka, H., Watanabe, D., Machida, C. & Machida, Y. The ACR4 receptor-like kinase is required for surface formation of epidermis-related tissues in *Arabidopsis thaliana*. *Plant J.* **39**, 298–308 (2004).
20. Gifford, M. L., Robertson, F. C., Soares, D. C. & Ingram, G. C. ARABIDOPSIS CRINKLY4 function, internalization, and turnover are dependent on the extracellular crinkly repeat domain. *Plant Cell* **17**, 1154–1166 (2005).
21. Cao, X., Li, K., Suh, S.-G., Guo, T. & Becraft, P. W. Molecular analysis of the CRINKLY4 gene family in *Arabidopsis thaliana*. *Planta* **220**, 645–657 (2005).
22. Meyer, M. R., Lichti, C. F., Townsend, R. R. & Rao, A. G. Identification of in vitro autophosphorylation sites and effects of phosphorylation on the *Arabidopsis* CRINKLY4 (ACR4) receptor-like kinase intracellular domain: insights into conformation, oligomerization, and activity. *Biochemistry* **50**, 2170–2186 (2011).
23. Zhao, Y., Liu, X., Xu, Z., Yang, H. & Li, J. Characterization and enzymatic properties of protein kinase ACR4 from *Arabidopsis thaliana*. *Biochem. Biophys. Res. Commun.* **489**, 270–274 (2017).
24. Qin, Y. *et al.* Redox-Mediated Endocytosis of a Receptor-Like Kinase during Distal Stem Cell Differentiation Depends on Its Tumor Necrosis Factor Receptor Domain. *Plant Physiol.* **181**, 1075–1095 (2019).

25. Nikonorova, N., Yue, K., Beeckman, T. & De Smet, I. Arabidopsis research requires a critical re-evaluation of genetic tools. *J. Exp. Bot.* **69**, 3541–3544 (2018).
26. Roeder, A. H. K., Cunha, A., Ohno, C. K. & Meyerowitz, E. M. Cell cycle regulates cell type in the Arabidopsis sepal. *Dev. Camb. Engl.* **139**, 4416–4427 (2012).
27. Xu, C. & Min, J. Structure and function of WD40 domain proteins. *Protein Cell* **2**, 202–214 (2011).
28. De Smet, I. *et al.* Receptor-like kinase ACR4 restricts formative cell divisions in the Arabidopsis root. *Science* **322**, 594–597 (2008).
29. Stahl, Y., Wink, R. H., Ingram, G. C. & Simon, R. A signaling module controlling the stem cell niche in Arabidopsis root meristems. *Curr. Biol.* **19**, 909–914 (2009).
30. Stahl, Y. & Simon, R. Peptides and receptors controlling root development. *Philos. Trans. R. Soc. Lond. B. Biol. Sci.* **367**, 1453–1460 (2012).
31. Berckmans, B., Kirschner, G., Gerlitz, N., Stadler, R. & Simon, R. CLE40 Signaling Regulates Root Stem Cell Fate. *Plant Physiol.* **182**, 1776–1792 (2020).
32. Stahl, Y. *et al.* Moderation of Arabidopsis root stemness by CLAVATA1 and ARABIDOPSIS CRINKLY4 receptor kinase complexes. *Curr. Biol. CB* **23**, 362–371 (2013).
33. Yue, K. *et al.* PP2A-3 interacts with ACR4 and regulates formative cell division in the Arabidopsis root. *Proc. Natl. Acad. Sci. U. S. A.* **113**, 1447–1452 (2016).
34. Meyer, M. R., Shah, S., Zhang, J., Rohrs, H. & Rao, A. G. Evidence for intermolecular interactions between the intracellular domains of the arabidopsis receptor-like kinase ACR4, its homologs and the Wox5 transcription factor. *PLoS One* **10**, e0118861 (2015).
35. Demko, V., Ako, E., Perroud, P.-F., Quatrano, R. & Olsen, O.-A. The phenotype of the CRINKLY4 deletion mutant of *Physcomitrella patens* suggests a broad role in developmental regulation in early land plants. *Planta* **244**, 275–284 (2016).
36. Nikonorova, N., Vu, L. D., Czyzewicz, N., Gevaert, K. & De Smet, I. A phylogenetic approach to study the origin and evolution of the CRINKLY4 family. *Front. Plant Sci.* **6**, 880 (2015).
37. Krissinel, E. & Henrick, K. Inference of macromolecular assemblies from crystalline state. *J. Mol. Biol.* **372**, 774–797 (2007).

38. Holm, L. & Sander, C. Protein structure comparison by alignment of distance matrices. *J. Mol. Biol.* **233**, 123–138 (1993).
39. Lim, D. *et al.* Crystal structure and kinetic analysis of beta-lactamase inhibitor protein-II in complex with TEM-1 beta-lactamase. *Nat. Struct. Biol.* **8**, 848–852 (2001).
40. Christie, J. M. *et al.* Plant UVR8 photoreceptor senses UV-B by tryptophan-mediated disruption of cross-dimer salt bridges. *Science* **335**, 1492–1496 (2012).
41. Rizzini, L. *et al.* Perception of UV-B by the *Arabidopsis* UVR8 protein. *Science* **332**, 103–106 (2011).
42. Pugalenthhi, G., Nithya, V., Chou, K.-C. & Archunan, G. Nglyc: A Random Forest Method for Prediction of N-Glycosylation Sites in Eukaryotic Protein Sequence. *Protein Pept. Lett.* **27**, 178–186 (2020).
43. Lau, K., Podolec, R., Chappuis, R., Ulm, R. & Hothorn, M. Plant photoreceptors and their signaling components compete for COP1 binding via VP peptide motifs. *EMBO J.* **38**, e102140 (2019).
44. Anne, P. *et al.* CLERK is a novel receptor kinase required for sensing of root-active CLE peptides in *Arabidopsis*. *Development* **145**, pii: dev162354 (2018).
45. Okuda, S. *et al.* Molecular mechanism for the recognition of sequence-divergent CIF peptides by the plant receptor kinases GSO1/SGN3 and GSO2. *Proc. Natl. Acad. Sci. U. S. A.* **117**, 2693–2703 (2020).
46. Stokes, K. D. & Gururaj Rao, A. Dimerization properties of the transmembrane domains of *Arabidopsis* CRINKLY4 receptor-like kinase and homologs. *Arch. Biochem. Biophys.* **477**, 219–226 (2008).
47. Stokes, K. D. & Rao, A. G. The role of individual amino acids in the dimerization of CR4 and ACR4 transmembrane domains. *Arch. Biochem. Biophys.* **502**, 104–111 (2010).
48. *Arabidopsis* Genome Initiative. Analysis of the genome sequence of the flowering plant *Arabidopsis thaliana*. *Nature* **408**, 796–815 (2000).
49. Rensing, S. A. *et al.* The *Physcomitrella* genome reveals evolutionary insights into the conquest of land by plants. *Science* **319**, 64–69 (2008).

50. Haruta, M., Sabat, G., Stecker, K., Minkoff, B. B. & Sussman, M. R. A peptide hormone and its receptor protein kinase regulate plant cell expansion. *Science* **343**, 408–411 (2014).
51. Kessler, S. A., Lindner, H., Jones, D. S. & Grossniklaus, U. Functional analysis of related CrRLK1L receptor-like kinases in pollen tube reception. *EMBO Rep.* **16**, 107–115 (2015).
52. Haruta, M., Gaddameedi, V., Burch, H., Fernandez, D. & Sussman, M. R. Comparison of the effects of a kinase-dead mutation of FERONIA on ovule fertilization and root growth of *Arabidopsis*. *FEBS Lett.* **592**, 2395–2402 (2018).
53. Chen, J. *et al.* FERONIA interacts with ABI2-type phosphatases to facilitate signaling cross-talk between abscisic acid and RALF peptide in *Arabidopsis*. *Proc. Natl. Acad. Sci. U. S. A.* **113**, E5519–5527 (2016).
54. Franck, C. M. *et al.* The Protein Phosphatases ATUNIS1 and ATUNIS2 Regulate Cell Wall Integrity in Tip-Growing Cells. *Plant Cell* **30**, 1906–1923 (2018).
55. Tanaka, H. *et al.* Novel receptor-like kinase ALE2 controls shoot development by specifying epidermis in *Arabidopsis*. *Development* **134**, 1643–1652 (2007).
56. San-Bento, R., Farcot, E., Galletti, R., Creff, A. & Ingram, G. Epidermal identity is maintained by cell-cell communication via a universally active feedback loop in *Arabidopsis thaliana*. *Plant J.* **77**, 46–58 (2014).
57. Cull, M. G. & Schatz, P. J. Biotinylation of proteins in vivo and in vitro using small peptide tags. *Methods Enzymol.* **326**, 430–440 (2000).
58. Fairhead, M. & Howarth, M. Site-specific biotinylation of purified proteins using BirA. *Methods Mol. Biol.* **1266**, 171–184 (2015).
59. Hashimoto, Y., Zhang, S. & Blissard, G. W. Ao38, a new cell line from eggs of the black witch moth, *Ascalapha odorata* (Lepidoptera: Noctuidae), is permissive for AcMNPV infection and produces high levels of recombinant proteins. *BMC Biotechnol.* **10**, 50 (2010).
60. Bojar, D. *et al.* Crystal structures of the phosphorylated BRI1 kinase domain and implications for brassinosteroid signal initiation. *Plant J.* **78**, 31–43 (2014).
61. Kabsch, W. Automatic processing of rotation diffraction data from crystals of initially unknown symmetry and cell constants. *J. Appl. Crystallogr.* **26**, 795–800 (1993).
62. Sheldrick, G. M. A short history of SHELX. *Acta Crystallogr. A* **64**, 112–122 (2008).

63. Bricogne, G., Vonrhein, C., Flensburg, C., Schiltz, M. & Paciorek, W. Generation, representation and flow of phase information in structure determination: recent developments in and around SHARP 2.0. *Acta Crystallogr. D Biol. Crystallogr.* **59**, 2023–2030 (2003).
64. Terwilliger, T. C. *et al.* Iterative model building, structure refinement and density modification with the PHENIX AutoBuild wizard. *Acta Crystallogr. D Biol. Crystallogr.* **64**, 61–69 (2008).
65. Murshudov, G. N., Vagin, A. A. & Dodson, E. J. Refinement of macromolecular structures by the maximum-likelihood method. *Acta Crystallogr. D Biol. Crystallogr.* **53**, 240–255 (1997).
66. Evans, P. Scaling and assessment of data quality. *Acta Crystallogr. D Biol. Crystallogr.* **62**, 72–82 (2006).
67. Lebedev, A. A. & Isupov, M. N. Space-group and origin ambiguity in macromolecular structures with pseudo-symmetry and its treatment with the program Zanuda. *Acta Crystallogr. D Biol. Crystallogr.* **70**, 2430–2443 (2014).
68. McCoy, A. J. *et al.* Phaser crystallographic software. *J. Appl. Crystallogr.* **40**, 658–674 (2007).
69. Emsley, P. & Cowtan, K. Coot: model-building tools for molecular graphics. *Acta Crystallogr. D Biol. Crystallogr.* **60**, 2126–2132 (2004).
70. Afonine, P. V. *et al.* Towards automated crystallographic structure refinement with phenix.refine. *Acta Crystallogr. D Biol. Crystallogr.* **68**, 352–367 (2012).
71. Goddard, T. D. *et al.* UCSF ChimeraX: Meeting modern challenges in visualization and analysis. *Protein Sci.* **27**, 14–25 (2018).
72. Karimi, M., De Meyer, B. & Hilson, P. Modular cloning in plant cells. *Trends Plant Sci.* **10**, 103–105 (2005).
73. Clough, S. J. & Bent, A. F. Floral dip: a simplified method for Agrobacterium-mediated transformation of *Arabidopsis thaliana*. *Plant J.* **16**, 735–743 (1998).
74. Dunnett, C. W. A Multiple Comparison Procedure for Comparing Several Treatments with a Control. *J. Am. Stat. Assoc.* **50**, 1096–1121 (1955).
75. Siegfried, S. & Hothorn, T. Count transformation models. *Methods Ecol. Evol.* **11**, 818–827 (2020).
76. Hothorn, T., Bretz, F. & Westfall, P. Simultaneous inference in general parametric models. *Biom. J.* **50**, 346–363 (2008).

77. Naismith, J. H., Devine, T. Q., Brandhuber, B. J. & Sprang, S. R. Crystallographic evidence for dimerization of unliganded tumor necrosis factor receptor. *J. Biol. Chem.* **270**, 13303–13307 (1995).
78. Notredame, C., Higgins, D. G. & Heringa, J. T-coffee: a novel method for fast and accurate multiple sequence alignment1. *J. Mol. Biol.* **302**, 205–217 (2000).
79. Kabsch, W. & Sander, C. Dictionary of protein secondary structure: pattern recognition of hydrogen-bonded and geometrical features. *Biopolymers* **22**, 2577–2637 (1983).
80. Davis, I. W. *et al.* MolProbity: all-atom contacts and structure validation for proteins and nucleic acids. *Nucleic Acids Res.* **35**, W375-383 (2007).

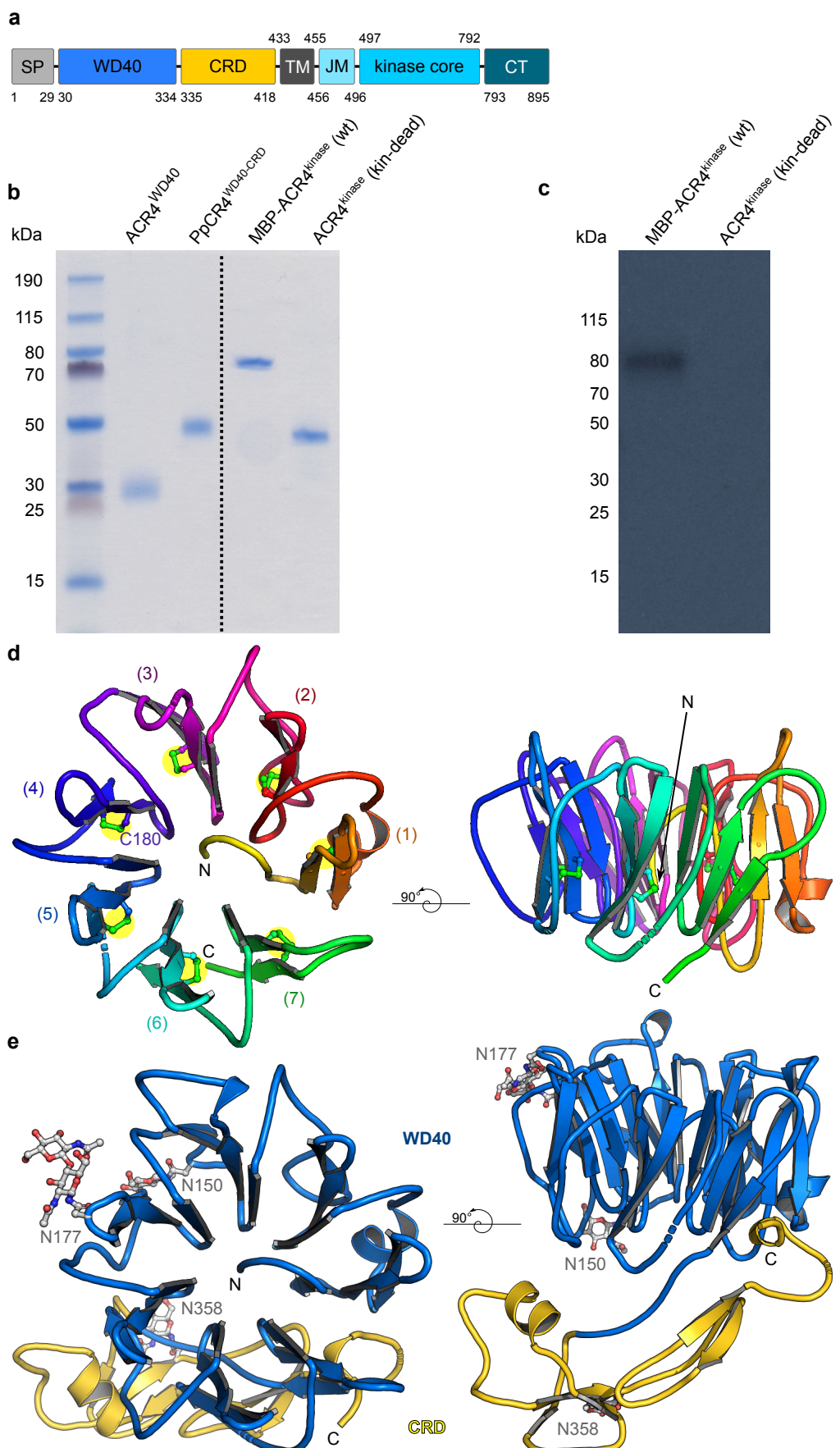


Figure 1. CRINKLY 4 receptor kinases harbor structurally unique β -propeller and cysteine-rich domains.

a, ACR4 domain scheme: SP, signal peptide; WD40, WD40 domain; CRD, cysteine-rich domain; TM, transmembrane helix; JM, juxtamembrane region; CT, C-terminal tail. **b**, SDS-PAGE analysis of purified CRINKLY4 proteins expressed in insect cells. **c**, Autoradiography *in vitro* kinase assay of the wild-type ACR4 kinase domain fused to maltose-binding protein (MBP), and of the unfused kinase domain carrying a point mutation (Asp659Asn) in the active site. The coomassie-stained gel loading control is shown in **b** (lanes on the right of the dotted line). **d**, Ribbon diagrams of ACR4^{WD40} in two orientations and colored from N- (yellow) to C-terminus (green). Disulfide bonds are shown in bonds representation and highlighted by yellow circles. **e**, Structure of PpCR4^{WD40-CRD} shown in two different orientation and colored in blue (WD40 domain) and yellow (CRD), respectively. The N-glycans visible in the electron density map are depicted in bonds representation (in gray).c++

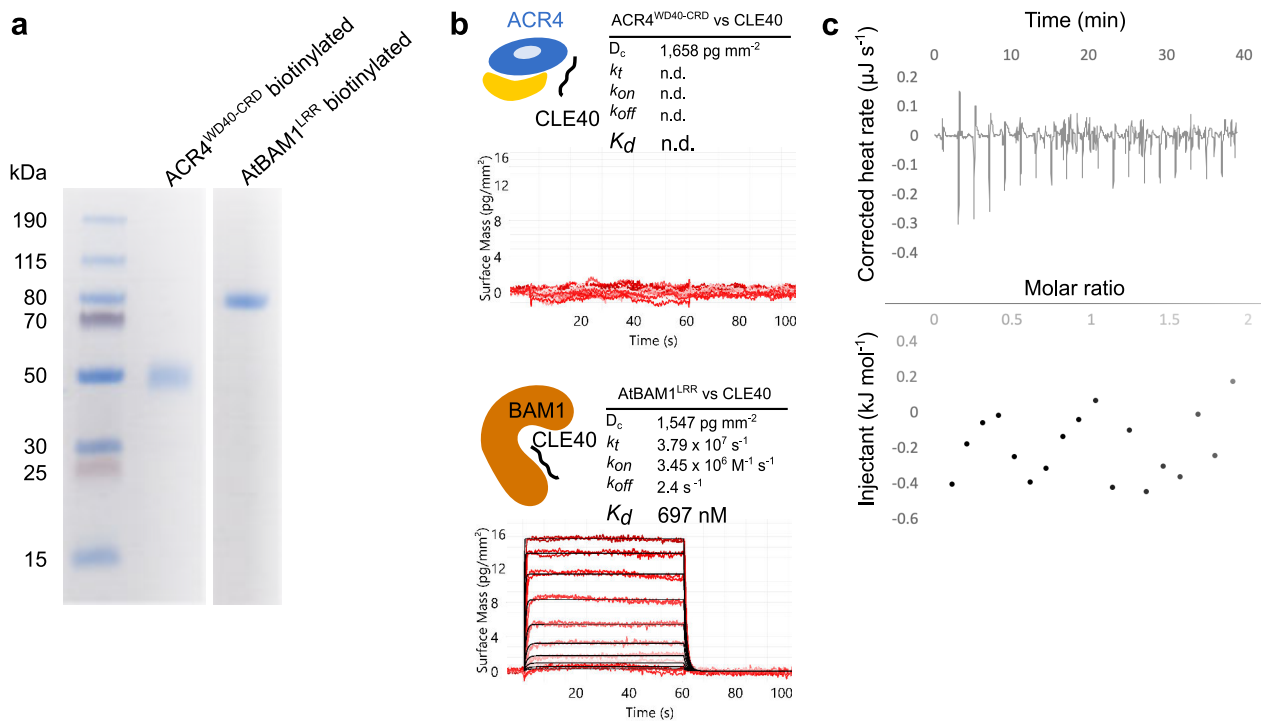


Figure 2. The ACR4 ectodomain does not bind the peptide hormone CLE40 in vitro.

a, SDS-PAGE analysis of the biotinylated ACR4^{WD40-CRD} and AtBAM1^{LRR} ectodomains used for binding experiments. **b**, Quantitative grating-coupled interferometry (GCI) binding assay of a synthetic CLE40 peptide versus ACR4^{WD-CRD} and BAM1^{LRR}. Shown are sensograms with raw data in red and their respective fits in black. Table summaries of kinetic parameters are shown alongside (D_c , density of captured protein; k_t , mass transport coefficient; k_{on} , association rate constant; k_{off} , dissociation rate constant; K_d , dissociation constant; n.d., no detectable binding, n=3). **c**, Isothermal titration calorimetry (ITC) experiment of ACR4^{WD-CRD} versus CLE40. No binding was detected in this assay (n=3).

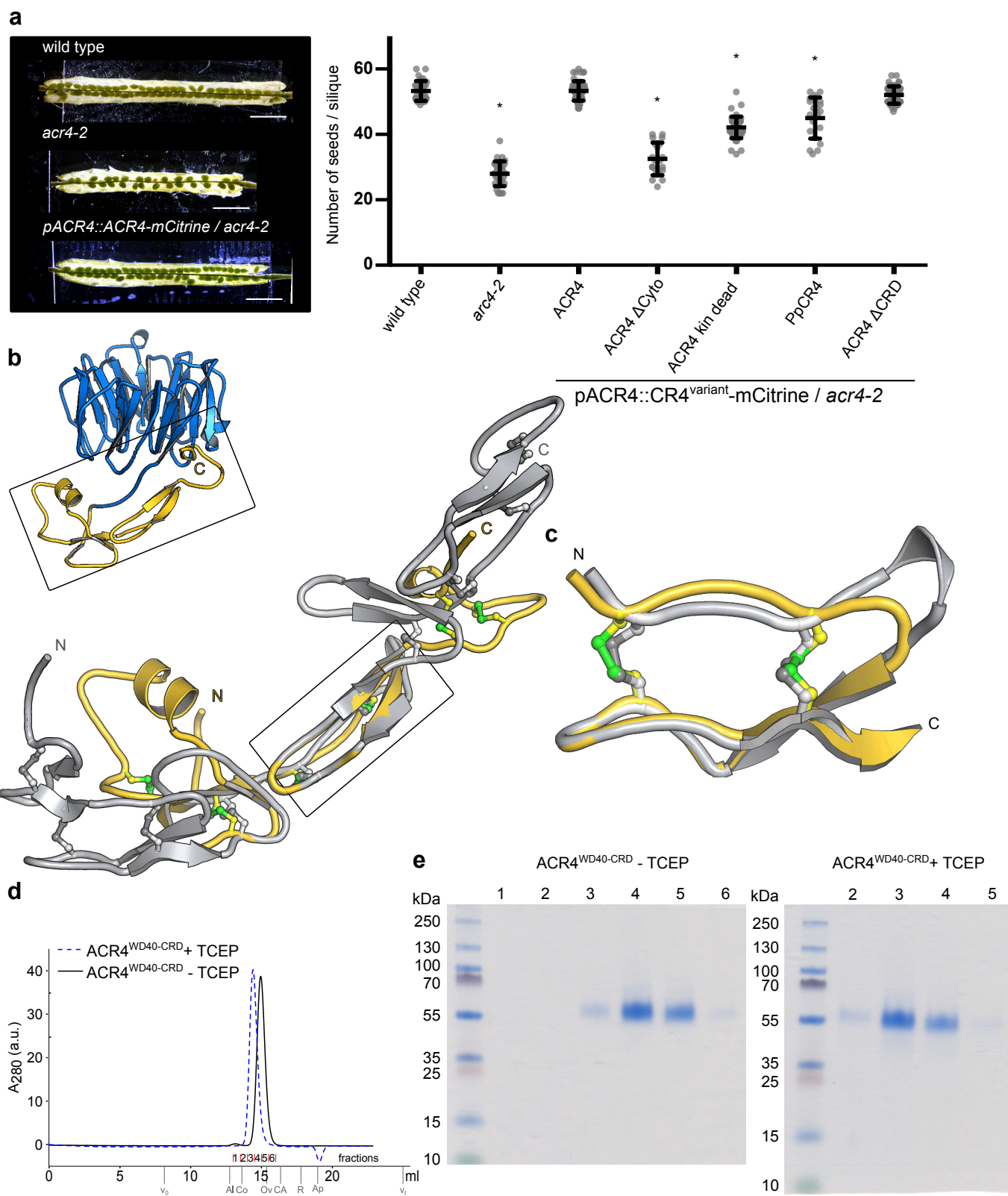


Figure 3. CRINKLY4 ectodomains harbor an evolutionary conserved function.

a, Reverse genetic rescue experiments of the seed filling phenotype of *acr4-2*. Left panel: Seed development phenotypes of wild type, *acr4-2* and a complemented line. Right panel: Ten siliques per transgenic line from three independent homozygous T3 lines were pooled and plotted as beeswarm plots with the bold line representing mean, whiskers indicating the standard deviation, and circles depicting the raw data. Seed counts per siliques significantly different from wild type were determined by simultaneous comparisons of several mutants against wild type using the Dunnett procedure (indicated by an asterisk). **b**, Ribbon diagram overview of PpCR4^{WD40-CRD} (colors as in Fig. 1) and close-up view of the CRD superimposed to a type I TNF receptor ectodomain (PDB-ID 1NCF⁷⁷; in gray). The six invariant disulfide bridges of CRINKLY4 CRDs are shown in green, the disulfide bonds in TNFR are shown in gray (in bonds representation). **c**, Superposition of the structurally homologous PpCR4^{CRD} (in yellow) and TNFR (in gray) core segments (r.m.s.d. is ~1 Å comparing 20 corresponding C_α atoms). **d**, Analytical size-exclusion chromatography of ACR4^{WD40-CRD} in the pre- or absence of Tris(2-carboxyethyl)phosphine (TCEP). Void (V₀), total (V₁), and elution volumes for molecular-mass standards (Al, Aldolase, 158 kDa; Co, Conalbumin, 75 kDa; Ov, Ovalbumin, 44 kDa; CA, Carbonic Anhydrase, 29 kDa; R, Ribonuclease A, 13.7 kDa; Ap, Aprotinin; 6.5 kDa) are indicated. **e**, SDS-PAGE analysis of fractions shown in d.

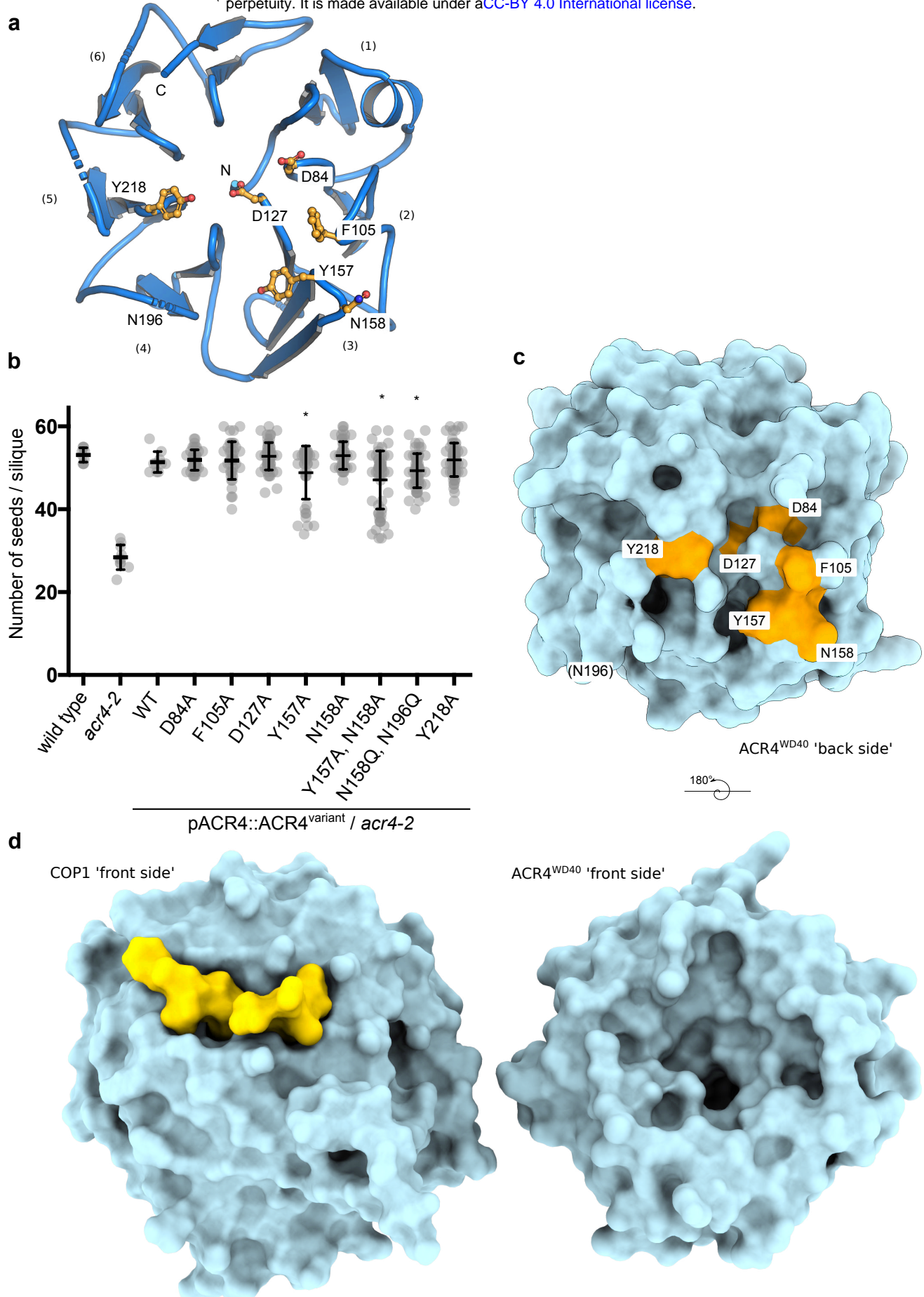
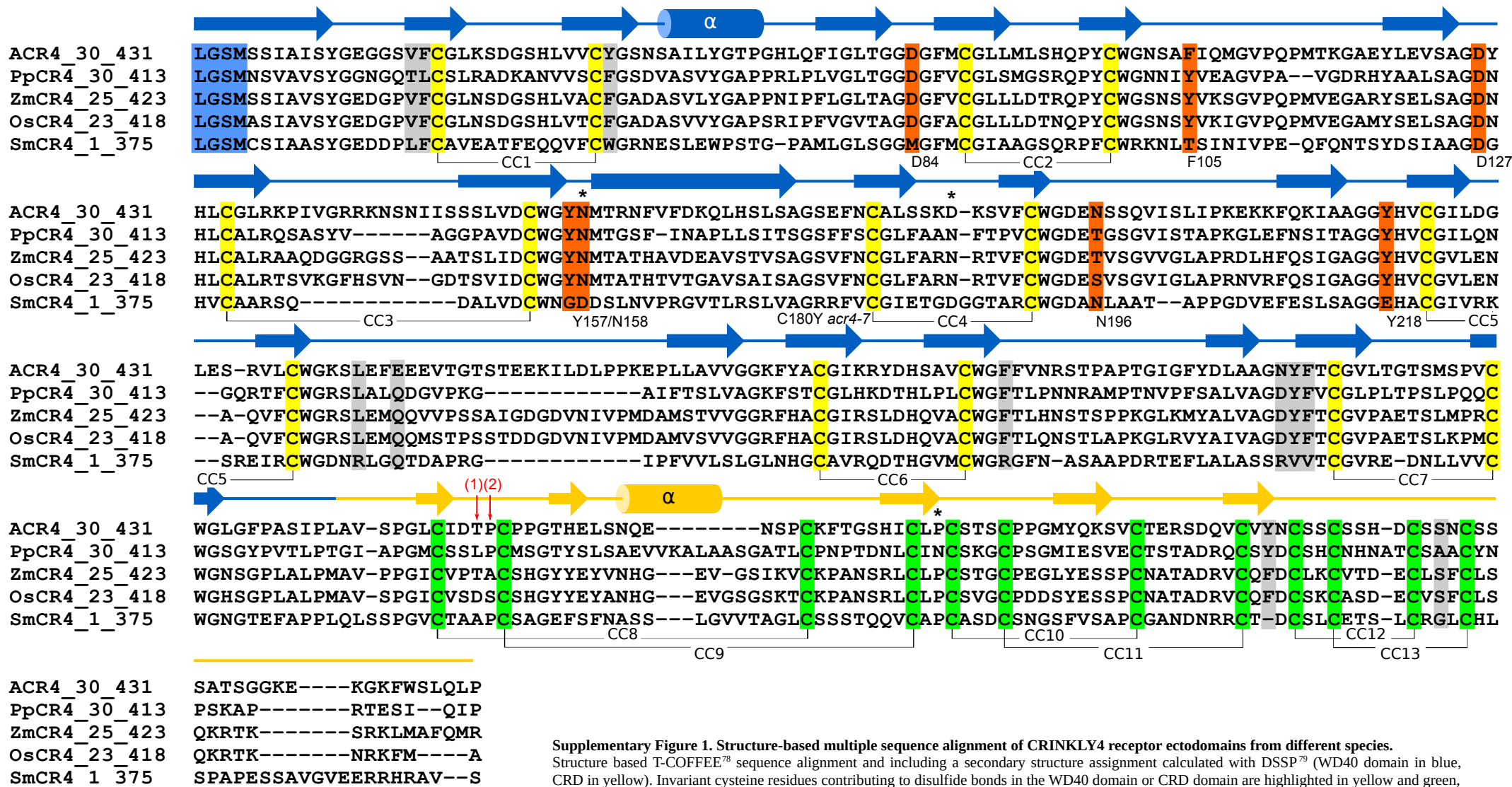


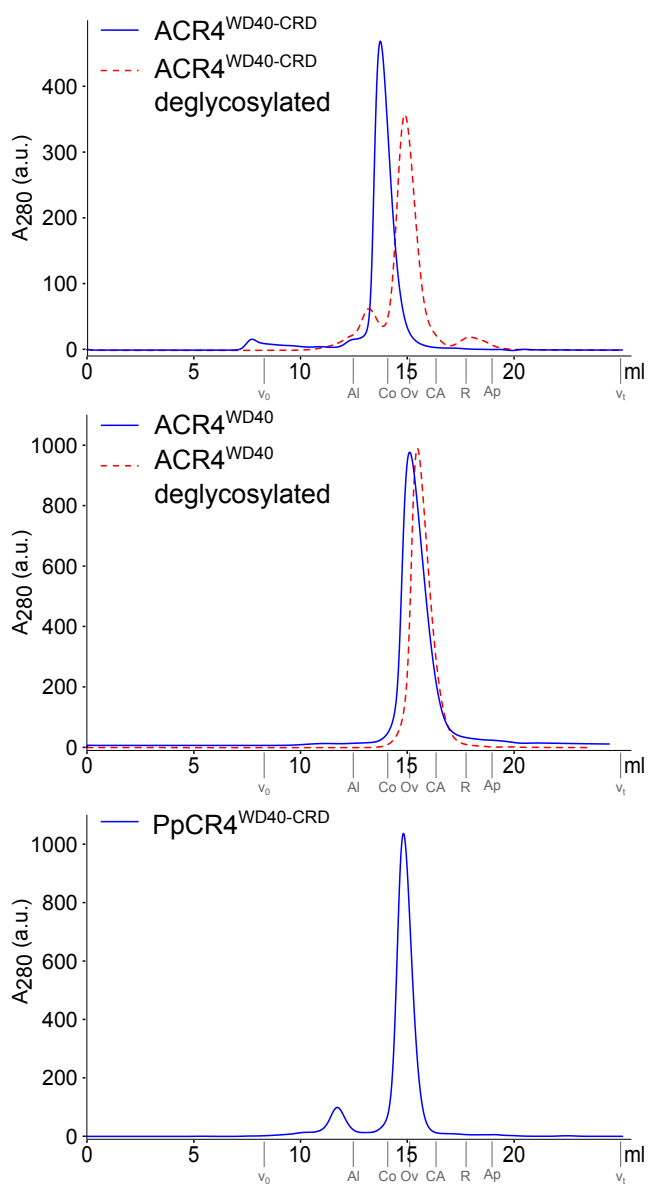
Figure 4. The CRINKLY4 WD40 domain contains a putative ligand binding groove.

a, Ribbon diagram of $ACR4^{WD40}$ (in blue) with surface exposed conserved residues shown in bonds representation (in orange) at the exposed surface. Blade numbers are indicated. **b**, Effect on surface point-mutations on $ACR4$ -mediated seed production. Ten siliques per transgenic line from three independent homozygous T3 complementation lines were pooled and plotted as beeswarm plots with the bold line representing mean, whiskers indicating the standard deviation, and circles depicting the raw data. The plots for wild type, $acr4-2$ and $ACR4$ were generated from same data sets shown in Fig. 3a. Seed counts per siliques significantly different from wild type were determined by simultaneous comparisons of several mutants against wild type using the Dunnett procedure (indicated by an asterisk). **c**, Molecular surface of the $ACR4^{WD40}$ β -propeller domain 'back side' (in light blue). The positions of the mutated residues are highlighted in orange. **d**, Comparison of the 'front sides' of the structurally related WD40 domains of COP1 (PDB-ID 6QTO⁴³ left panel) and ACR4 (right panel, r.m.s.d is ~ 3.5 comparing 205 corresponding C_{α} atoms). The COP1 VP-peptide ligand derived from the transcription factor HY5 is shown in yellow. Note the large and deep putative binding groove in the corresponding surface area in $ACR4^{WD40}$.



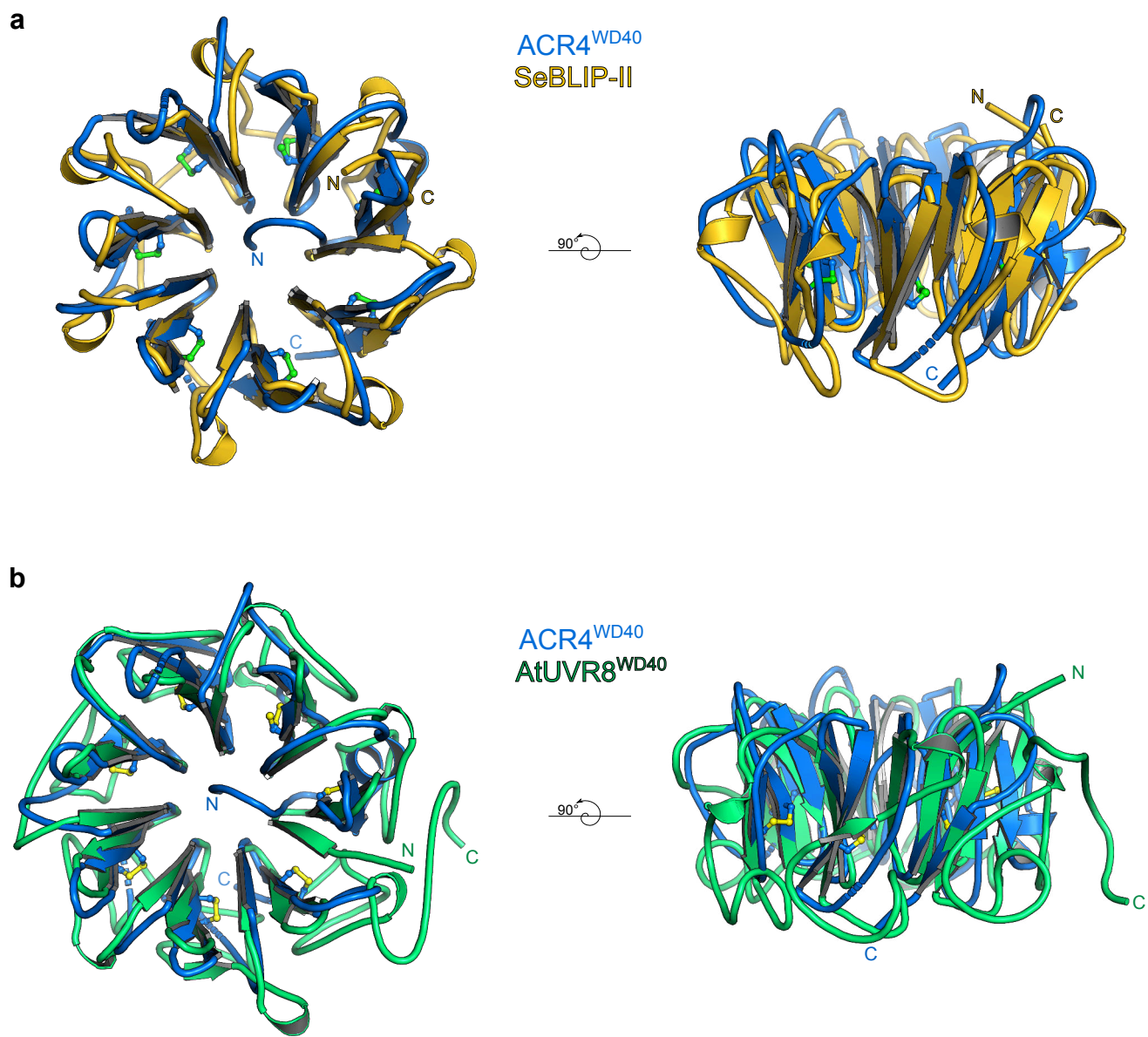
Supplementary Figure 1. Structure-based multiple sequence alignment of CRINKLY4 receptor ectodomains from different species

Structure based T-COFFEE⁷⁸ sequence alignment and including a secondary structure assignment calculated with DSSP⁷⁹ (WD40 domain in blue, CRD in yellow). Invariant cysteine residues contributing to disulfide bonds in the WD40 domain or CRD domain are highlighted in yellow and green, respectively. Residues analyzed with point mutations in this study are shown in orange. Conserved residues in the WD40 – CRD domain interface are depicted in gray. Asterisks denote the location of experimentally confirmed N-glycosylation sites. Red arrows represent domain boundaries for the TNFR/CRD deletion constructs in previous reports: (1)²⁴, (2)²⁰. ACR4 (*Arabidopsis thaliana*) UNIPROT-ID (<http://uniprot.org>) Q9LX29; PpCR4 (*Phycomitrella patens*) A9RKG8; ZmCR4 (*Zea mays*) O24585; OsCR4 (*Oryza sativa*) Q75J39; SmCR4 (*Selaginella moellendorffii*) D8T625. Note that the annotated SmCR4 sequence may be incomplete.



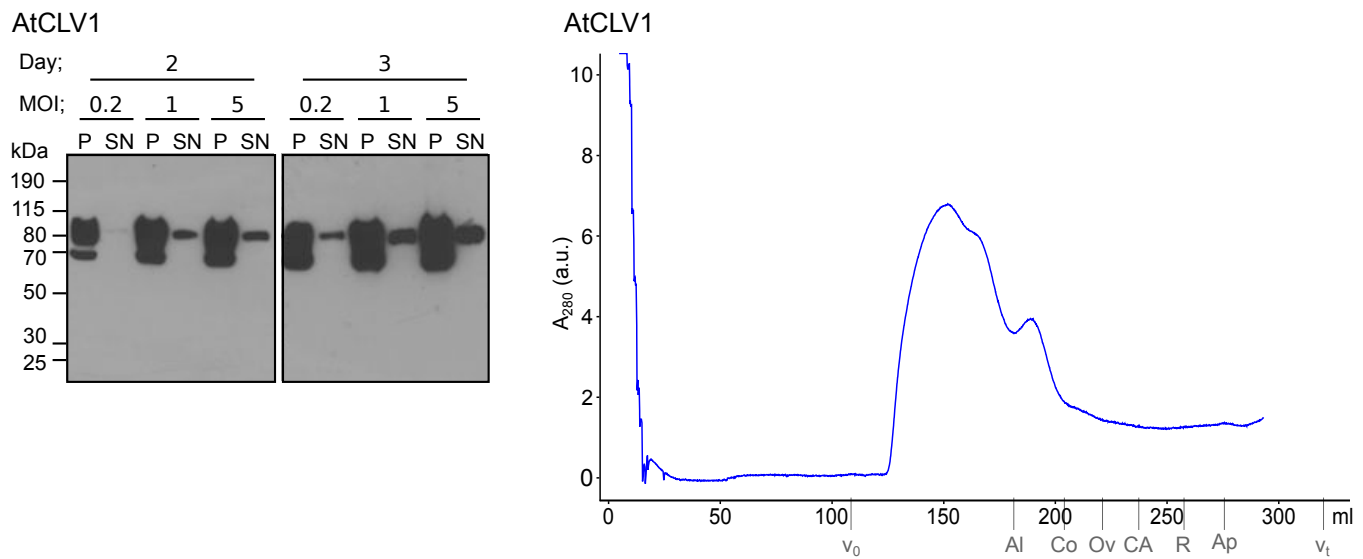
Supplementary Figure 2. CRINKLY4 receptor ectodomains behave as monomers in solution.

Analytical size-exclusion chromatography of the ACR4^{WD40-CRD}, ACR4^{WD40} and PpCR4^{WD40-CRD} in the presence or absence of enzymatic deglycosylation. The void volume (V₀), the total column volume (V_t), and the elution volumes for molecular-mass standards (Al, Aldolase, 158 kDa; Co, Conalbumin, 75 kDa; Ov, Ovalbumin, 44 kDa; CA, Carbonic Anhydrase, 29 kDa; R, Ribonuclease A, 13.7 kDa; Ap, Aprotinin; 6.5 kDa) are indicated.



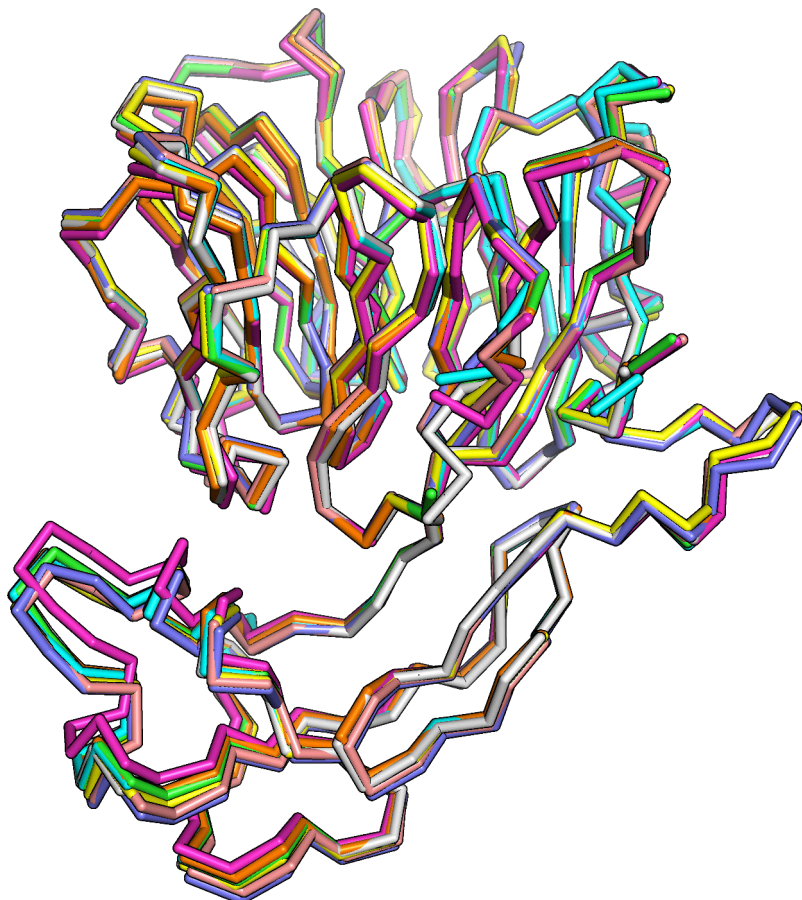
Supplementary Figure 3. ACR4^{WD40} shares structural features with known WD40 domains.

Structural superposition of ACR4^{WD40} (blue ribbon diagram) with **a**, the secreted β -lactamase inhibitor protein II BLIP-II (PDB-ID 1JTD³⁹, in yellow) from the bacterium *Streptomyces exfoliatus* (r.m.s.d. is ~ 2.2 Å comparing 192 corresponding C_α atoms), and **b**, with the WD40 domain of the UV-B photoreceptor UVR8 (PDB-ID 4D9S⁴⁰, r.m.s.d. is ~ 2.4 Å comparing 218 corresponding C_α atoms). Note that SeBLIP-II and UVR8 shares the blade number and overall architecture with ACR4^{WD40}, but lack the buried N-terminal strand and the conserved disulfide bonds stabilizing each blade.



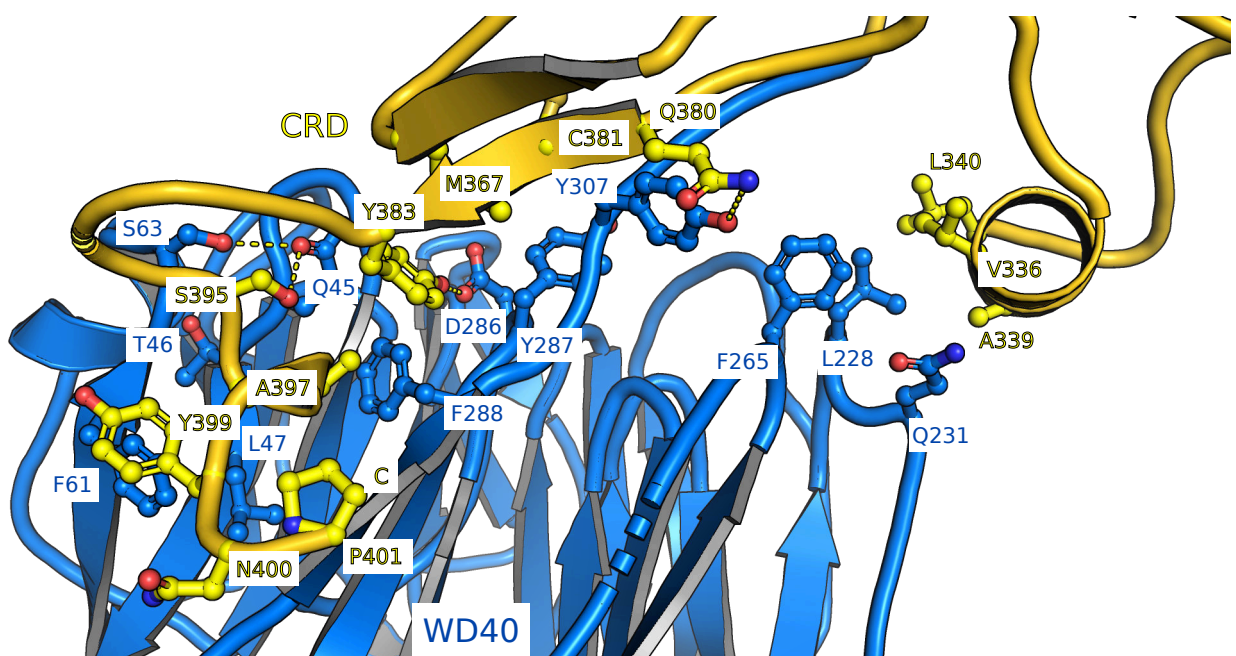
Supplementary Figure 4. Expression and purification attempts of the AtCLV1 LRR ectodomain.

Shown are immunoblot analyses monitoring the secreted expression of the AtCLV1 ectodomain (see Methods) with an anti-His antibody (left panels, Day, days post infection, MOI, multiplicity of infection; SN, supernatant; P, pellet). Right panel: Preparative size-exclusion chromatography of the purified AtCLV1 ectodomain reveals the presence of large aggregates. The void (V_0), total (V_t), and elution volumes for molecular-mass standards (AI, Aldolase, 158 kDa; Co, Conalbumin, 75 kDa; Ov, Ovalbumin, 44 kDa; CA, Carbonic Anhydrase, 29 kDa; R, Ribonuclease A, 13.7 kDa; Ap, Aprotinin; 6.5 kDa) are indicated.



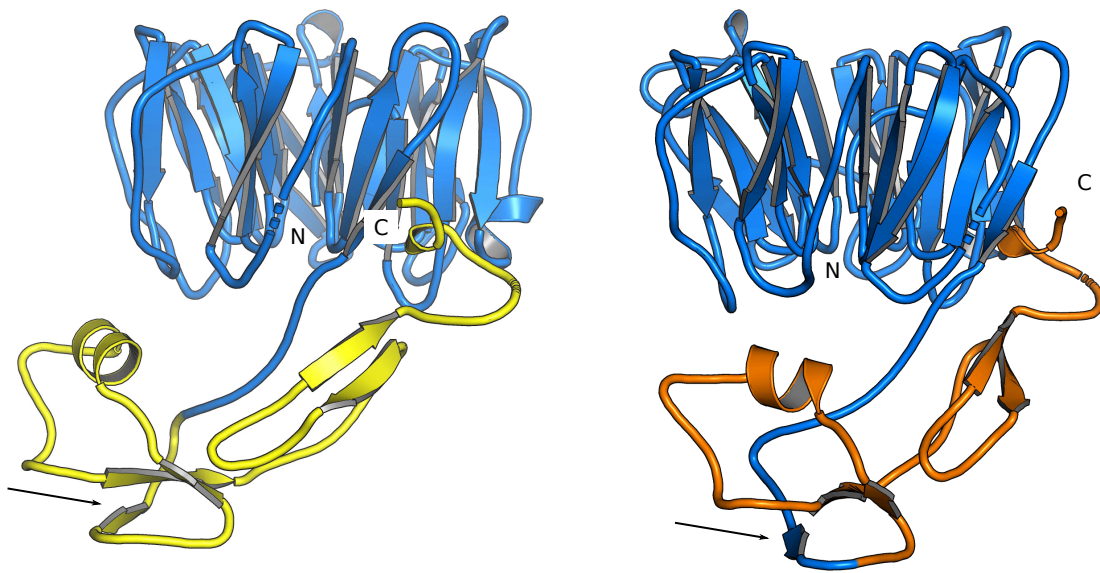
Supplementary Figure 5. Only small WD40 - CRD inter-domain movements can be observed in the PpCR4 crystal structure.

Structural superposition of the eight molecules located in the asymmetric unit of the PpCR4^{WD40-CRD} crystal structure (r.m.s.d. is ~0.3-0.5 Å comparing 360 corresponding C_α atoms). Individual molecules are shown in different colors as C_α traces.



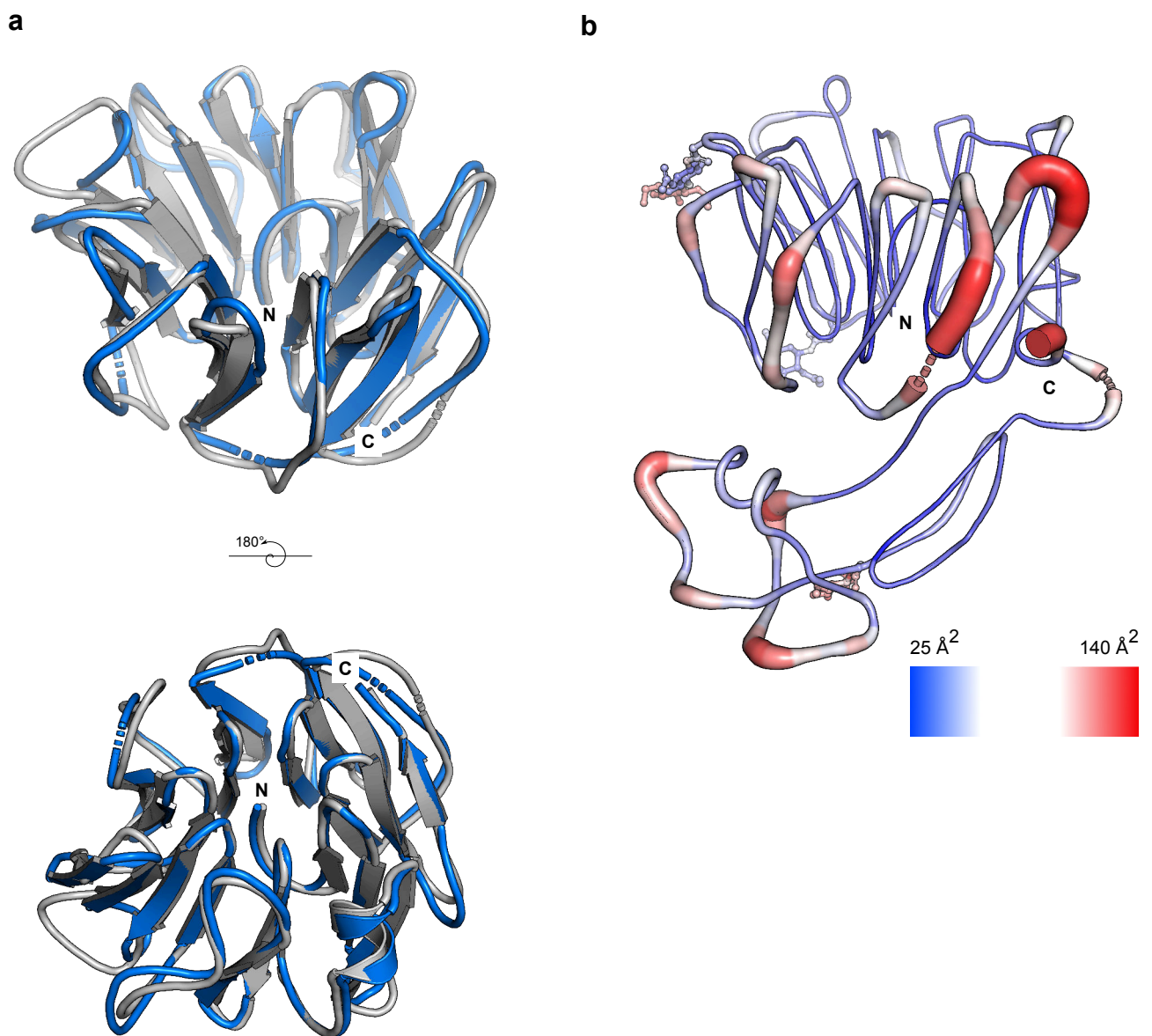
Supplementary Figure 6. Overview of the WD40 – CRD domain interface in the PpCRD^{WD40-CRD} structure.

Shown is a ribbon diagram of the PpCR4 ectodomain (colored according to Fig. 1e) with selected interface residues shown in bonds representation. Hydrogen bonds and salt bridges are indicated by dotted lines.



Supplementary Figure 7. Structural visualization of the TNFR/CRD domain boundaries used in this and in previous studies.

Ribbon diagram of PpCR4^{WD40-CRD} with the WD40 domain shown in blue and the experimentally determined CRD domain boundaries shown in yellow (left panel). The previously used TNFR domain boundaries^{20,24} derived from sequence analysis (in orange) omit the most N-terminal β-strand in the CRD (in blue, indicated by a black arrow).



Supplementary Figure 8. Structurally conserved loop regions contribute to the formation of a putative ligand binding groove in CRINKLY4 WD40 domains.

a, Structural superposition of the isolated WD40 domain from ACR4 (blue) and PpCR4 (light gray, r.m.s.d. is ~ 1.4 Å comparing 246 corresponding C_α atoms) reveals the loop regions contributing to the formation of a putative ligand binding groove to adopt similar orientations in both structures. **b**, A temperature (B-) factor plot of PpCR4^{WD40-CRD} (molecule chain A) reveals little structural flexibility for the secondary structure elements forming part of the putative binding groove, while the partially disordered loops connecting the blades of the β-propeller and the loops connecting the CRD appear mobile in the PpCR4^{WD40-CRD} crystal structure.